Building and Environment 213 (2022) 108807

Contents lists available at ScienceDirect

Building and Environment

journal homepage: www.elsevier.com/locate/buildenv

Digital twin models for optimization and global projection of building-integrated solar chimney

Rasikh Tariq [a,*], C.E. Torres-Aguilar [b], J. Xamán [b,1], I. Zavala-Guillén [c], A. Bassam [a], Luis J. Ricalde [a], O. Carvente [a]

[a] Facultad de Ingeniería, Universidad Autónoma de Yucatán, Av. Industrias No Contaminantes por Anillo Periférico Norte, Apdo. Postal 150, Cordemex, Mérida, Yucatán, Mexico

[b] Tecnológico Nacional de México/CENIDET, Prol. Av. Palmira S/N. Col. Palmira, Cuernavaca, Morelos, CP. 62490, Mexico

[c] Laboratorio de Energías Renovables, Departamento de Electrónica y Telecomunicaciones, División de Física Aplicada, Centro de Investigación Científica y de Educación Superior de Ensenada, CICESE, Carretera Ensenada Tijuana No. 3918, Zona Playitas, Ensenada, Baja California, CP 22860, Mexico

ARTICLE INFO

Keywords:
Thermal management
Passive cooling
Artificial intelligence
Solar chimney
Optimization
Global projection
Sustainability

ABSTRACT

Current research on solar chimneys has focused on developing regression-based empirical models, which might not be correct enough compared to the soft computing tools i.e., techniques of artificial intelligence. Current research has also published the search algorithm-based single-objective optimization of solar chimneys, whereas the latest genetic algorithm-based multi-objective optimization can be more useful for decision-making purposes. Current research has also not focused on the macro or global impact of the usage of solar chimneys in context with the energy, economic, environmental, social, and political framework of the world. This research fills these gaps by the development of a digital twin model of the solar chimney using a multivariate regression model based on the least square method and an artificial intelligence (AI) method based on multilayer perceptron artificial neural network (MLP-ANN) and their comparison. A multiobjective optimization study along with the application of Technique for Order of Preference by Similarity to Ideal Solution (TOPSIS) is applied to optimize the geometric dimensions of the solar chimney considering four different climatic zones using an elitist non-dominated sorting genetic algorithm (NSGA-II) to maximize the number of air changes per hour, energy efficiency, and specific environmental influence. The results have shown that the statistical performance indicators like the coefficient of regression, etc., are higher for the MLP-ANN technique as compared to the multivariate regression method, thus, the AI technique is preferred. Comparison of optimization results with the base case condition has shown that the number of air changes can be improved between ~71% and 87%. The global projection has demonstrated that the integration of solar chimneys in low-income countries with high air-conditioners installation rates must be necessary. It is also recommended to use solar chimneys in high-income countries for the renovation of the existing built environment to decrease the energy intensity of the building sector.

1. Introduction

World Green Building Council has outlined that the green buildings can improve the lives of billions and helps to achieve the sustainable development goals of the United Nations [1] especially no. 3: good health and well-being, no. 7: affordable and clean energy, no. 8: decent work and economic growth, no. 9: industry, innovation, and infrastructure, no. 11: sustainable cities and communities, no. 12: responsible consumption and production, no. 13: climate action, no. 15: life on land, and no. 17: partnerships for the goals. Better and sustainable design of the buildings can also avoid the sick building syndrome [2] resulting from poor indoor quality caused by inadequate ventilation, fluctuations in temperature, and inadequate humidity levels. The role of buildings has also grown up to be more significant in the COVID-19 pandemic especially when the latest research has correlated the association of COVID-19 infection rates with the poor ventilation design of the buildings [3–5]. On the other hand, the COP23 climate change conference held in Bonn, Germany has declared that the urban areas account for

* Corresponding author.
E-mail addresses: rasikhtariq@gmail.com, rasikhtariq@alumnos.uady.mx (R. Tariq).

[1] This work is dedicated with love to the departed soul of Professor Jesús Perfecto Xamán Villaseñor (academically known as J. Xamán).

https://doi.org/10.1016/j.buildenv.2022.108807
Received 5 November 2021; Received in revised form 13 January 2022; Accepted 16 January 2022
Available online 21 January 2022
0360-1323/© 2022 Elsevier Ltd. All rights reserved.

between 37–49% of the global greenhouse gas emissions and buildings alone are responsible for some 40% of global environmental emissions [6]. These numbers are also quite similar to the global share of building energy consumption which is expected to rise to 50% by mid-decade if no betterment steps are taken in this sector. It is estimated that HVACR (Heating, Ventilating, Air Conditioning, and Refrigeration) is only responsible for 50–60% of the energy share within the residential building. Thus, it is necessary to look for energy cheap alternatives for better thermal management of the buildings.

Generally, there could be two broad steps in the attainment of energy efficiency in the buildings [7,8]. The first one is the renovation of the buildings which includes the usage of better components of the building envelope and passive components. The second one would be the decarbonization of an already renovated building which can be attained through the usage of energy-efficient equipment and renewable energy integrated systems. Passive components of the building are energy-efficient and eco-friendly alternatives that can improve the thermal comfort conditions of the built environment with little or almost negligible energy consumption. It is estimated that the usage of passive components can decrease the thermal load of the building by around 40% which can be a considerable gain provided it can be implemented on a mass scale. The usage of preventive techniques, and modulation and heat dissipation techniques constitute the passive systems. The prevention techniques include the usage of solar control [9], thermal insulations [10]v, control of internal gain, and layout of building architecture. The modulation and heat dissipation techniques allow the building to store and dissipate heat gain through the transfer of heat from the source/sink to the climate which can be attained through the usage of a thermal mass i.e., phase changing material [11,12], and through free cooling methods like night flushing, evaporative cooling [13], geothermal cooling/heating [14], natural ventilation, and double-skin façade [15]. Double-skin façade technology especially the usage of the solar chimney [16] can take around 50% of the building's energy load while working through the usage of only incoming solar radiation.

Extensive research is available on the size, operation, optimality, sensitivity, and orientation of the solar chimney. Sivalakshmi et al. [17] evaluated the thermal performance of a wall solar chimney integrated with a room for warm and humid conditions. The authors obtained the highest air velocity of 0.6 m/s and a maximum temperature variation between the outlet and inlet of the solar chimney of 5.8 °C. Zhang et al. [18] reported the performance of a solar chimney for a multizonal building while considering various configurations and external environmental conditions. The authors concluded that the velocity distribution of the long and narrow room layout shows an average improvement of 2.5% as compared to a room with a significant difference in width. Vazquez-Ruiz et al. [19] studied the effect of solar roof chimney position on the heat transfer characteristics of the room. The authors concluded that the solar chimney offers the best use of natural ventilation by offering efficient, economical, and ecological manner to improve the thermal comfort conditions. Cao et al. [20] used a single solar chimney technology as a natural free ventilator option for a case study of Hong Kong. The authors reported that the energy-saving performance of the solar chimney with a tilted angle of 20° is around 144% higher than a solar chimney with other tilt angles. He et al. [16] provided the ventilation performance of a solar chimney in a test house through field measurement. Soto et al. [21] simulated and experimentally studied a wind tower assisted by a solar chimney for residential buildings for the location of Murcia, Spain. The authors concluded that the results could contribute to increasing the awareness of the role those passive strategies can play to achieve the goals set by the European Union to meet certain energy efficiency standards of the buildings. Villar-Ramos et al. [22] provided a parametric analysis of the thermal behavior of a single channel solar chimney and concluded that the passive ventilation system can attain a maximum number of air changes per hour of 27.11 1/h.

Currently, there is also a list of innovative applications of solar chimneys. For example, Salari et al. [23] integrated the solar chimney with a photovoltaic module and a phase-changing material. The authors demonstrated that the usage of this combination can be the best option for residential buildings. Cao et al. [24] provided an innovative integration of a solar chimney with a solar panel and a phase-changing material and tested it for transient weather conditions of Hong King. The authors concluded that the usage of such a configuration has economic benefits in the month of June by saving 2.88 dollars per month. Cao et al. [11] also provided a comprehensive optimization of phase-changing material in a hybrid application with solar chimney and solar panels to provide power and air ventilation. Pouranian et al. [25] integrated the solar chimney with an earth-to-air heat exchanger applied on a hot-arid climatic zone and reported that an enhancement of up to 175% can be achieved in a number of air changes per hour. Wang et al. [26] combined a solar chimney with a water wall for the buildings and it was concluded that the ventilation rate and the room temperature obtained with a solar chimney in front of the water wall are higher than a single solar chimney and the configuration water wall in front of the solar chimney is preferred. Li et al. [27] provided the passive ventilation and cooling performance with an integrated solar chimney and earth-to-air heat exchanger and concluded that the combination can provide natural ventilation for the whole day. Some interesting applications are also presented by Shi et al. [28], and Cheng et al. [29,30] where the authors proposed using the solar chimney for the natural ventilation and smoke exhaustion in the case of a fire inside the building.

Very few studies are available on the optimization of solar chimneys. Most optimization studies are based upon parametric studies where an optimized solution is evaluated by searching the local minima or maxima for only a single objective function. In reality, it is always better to consider various indicators like cost, dimensions, and operational performance in the optimization study which was seen to be absent in the literature. For example, Zhu et al. [31] provided a coupling optimization of key influencing factors on the PCM Trombe wall. The considered design variables were air gap, thermal storage wall, double-layer PCM wallboard, and external sun shading device to find the optimum energy consumption of the system. The authors used an optimization program called GenOpt coupled with TRNSYS software by implementing a search-based algorithm called Hooke Jeeves. This is a single objective optimization study where the significance of the results is not useful for the decision-makers who also need a perspective on other performance indicators of the solar chimney. Furthermore, the search-based optimization algorithm is generally less efficient than the heuristic-based algorithms and can also fall in local optima. Ma et al. [32] provided optimization of the energy performance of ventilated composite Trombe wall for winter heating applications. The optimization is actually the physical modification in the solar chimney where the authors modified the layer of a closed cavity to a ventilated air cavity of the composite Trombe-Michel wall. The authors studied the effects of controlling airflow from the ventilated air layer to the indoor and the operation of the fans. Serageldin et al. [33] developed a parametric study and optimization of a solar chimney passive ventilation system coupled with an earth-to-air heat exchanger. The authors have simulated the configuration on ANSYS and mentioned that the software has two techniques to conduct the optimization: response surface optimization, and direct optimization. The authors optimized eight design parameters which include: width, air gap, inclination angle, length, and position of the solar chimney, and inlet height, pipe diameter, and position of the earth-air heat exchanger. Later in the document, the authors have mentioned using the multiobjective genetic algorithm to obtain the optimization results of the aforementioned variables with respect to solar radiation, wind velocity, and ambient temperature. However, the optimization study shown by the authors does not exhibit different or conflicting objective functions for the optimization study. In fact, the study is originally focused on the CFD study and there are also no details on the integration of the optimization algorithm with the developed CFD

model. Furthermore, the authors have not shown any Pareto front to apply other multicriteria decision-making tools depending upon the constraints of the policymaker to select the optimal point among all other non-dominating optimal points. This study also misses the influence of changing climatic conditions on the optimized performance of the integrated configuration of the solar chimney and earth-air heat exchanger. Thus, the gaps in the literature have shown that further optimization studies are mainly required by using heuristic algorithms for multiobjective optimization purposes.

Another perspective in the research of solar chimneys is the necessity of developing alternate empirical correlations for the performance indicators of the solar chimney. They are helpful for applied applications because of their availability to provide a rapid response without the solution of any iterative CFD or analytical model. One such search is published by Shi et al. [34] where the authors have developed an empirical model to predict the performance of the atypical solar chimney. The authors have concluded that the room size including the height, width, and the length of the room along with the opening location has a limited influence on the performance. The authors have also concluded that the radiation from hot walls can be ignored. Using a regression fit, the authors have proposed a proportional relationship of the airflow rate under thermal buoyancy-driven by temperature differences for space with two different heights. It included the variables like the area of the opening, inlet, outlet, hot wall, heat transfer coefficient, chimney height, and surface temperature. The developed correlation has shown conformity with the experimental data. Even though the technical details of the regression model are not presented. However, in general, it is based upon the statistical technique. The statistical techniques are strong enough to predict the performance of a system however, now the usage of the techniques of artificial intelligence can provide a much better prediction model. Thus, as outlined, there is also a need for further research to develop more accurate empirical models of the solar chimney, especially, a comparison between the statistical regression method and an artificial intelligence-based method that can be quite useful.

Another gap identified in the literature is related to the influence of different weather conditions on the performance of the solar chimney. Salehi et al. [35] performed a thermal comfort efficacy of solar chimneys for different weather conditions including hot and humid, hot and arid, mild and humid, and cold and humid. Jamali et al. [36] reported the thermal and economic assessment of solar chimney cooled semi-transparent solar panel plants for different climatic zones. Hernández-López et al. [37] provided the thermal behavior of a room with a solar chimney for ventilation purposes for the tropical wet climatic zone of southeast Mexico. Jiménez-Xamán et al. [38] also reported the thermal performance of a rooftop solar chimney attached with a single room for the summer and winter conditions in Merida (tropical climatic zone). Nevertheless, more research is required to report a generalized optimized performance of a solar chimney for various climatic zones.

Thus, based on these identified gaps in the literature, this work aims to optimize the performance of a sun-facing wall attached vertically oriented conventional solar chimney integrated with a building based upon multicriteria (ventilation rate, energy efficiency, and environmental footprints) for various climatic zones. The work also provides a comparative assessment between conventional statistical-based empirical models and modern artificial intelligence techniques. Finally, another real contribution of this work is to globally project the performance of solar chimneys and correlate them with various social, economic, energetic, political, and environmental problems of the countries. This last step would be helpful for the policymakers at the government and international level in how the usage of passive components, i.e., solar chimneys, can help to develop a sustainable future. The research contribution of this work can also be summarized in a bullet wise manner, as follows:

I. Current research has utilized the whole building energy simulation packages to simulate the integration of a solar chimney with a building, but it requires the usage of such a dedicated tool for analysis purposes. On the other hand, the global energy balance model normally ignores the influence of the building characteristics on the performance of the solar chimney. Computational fluid dynamics-based models are complete, but it becomes computationally expensive to evaluate the optimal configurations. Thus, one of the research contributions of this work is the development of a physical model of the solar chimney integrated with the building characteristics using a holistic approach representing computationally economic package as compared to the usage of whole building energy simulation packages.
II. Current research has also focused on the usage of simplified models of solar chimneys using multivariate regression methods, but they are not extensively described in terms of the ANOVA (**AN**alysis **O**f **VA**riance) analysis, and compliance of the error assumptions, specially normality, independence, and homoscedasticity. In this way, one research contribution of this work is also to outline the limitations of the simplified models especially by the usage of multivariate regression method evaluated using the least square method.
III. Alternative to the multivariate regression method, one of the research contributions of this work is to recommend the usage of an artificial neural network as an alternative digital twin (simplified models) of the building-integrated solar chimney which also complies with the error assumptions.
IV. Current research on this area has extensively presented optimization packages to evaluate the best geometric characteristics of the solar chimney, especially based upon computational fluid dynamics results. However, the majority of this research targets only one objective function and relies on conventional computationally expensive search-based algorithms. Thus, another research contribution of this work is to use and apply a genetic algorithm-based optimization algorithm for multicriteria decision-making including ventilation, energy, and environmental profile of the system.
V. Current research has also detailed the sensitivity of different parameters on the performance indicators mainly based upon a parametric analysis in which the variable of interest is changed, and its influence is noted on the performance indicators. This work utilizes a simplified and innovative alternative to the sensitivity analysis based upon the Garson method [39] which directly provides the sensitivity of weight percentage of each variable of interest on the performance indicator by considering uncertainty in the variable of interest.
VI. Apart from the technical contribution of this research, this work projects the performance of the building-integrated solar chimney on a global scale and correlates it with certain political, legislative, social, economic, and environmental global problems. Such a type of interlinkage, in a lumped and holistic way, demonstrates the global benefits which can be obtained through the usage of the solar chimney in buildings for their thermal management.

2. Research method

The research method consists of a stepwise procedure starting from the physical model to the optimization process which is comprehensively explained in the subsequent sections.

2.1. Physical model of building-integrated solar chimney

Solar chimneys are double-skin façade passive components of the building which is used to meet an adequate ventilation rate of the building. The outer skin consists of a glass, an air channel, and an

absorber plate which is attached to the inner skin of the façade. The incoming solar radiation is transmitted from the glass cover is absorbed by the absorber plate increasing the temperature of the air in the passage between the glass and the wall. This increase in temperature causes a pressure difference increasing the upward suction velocity of the air which causes a suction with the building-integrated opening of the solar chimney. In this way, the air from the room passes the solar chimney through natural ventilation and takes away the heat of the built environment which helps the building to regulate its temperature. Fig. 1a shows the experimental buildings with a solar chimney installed on a sun-facing wall.

It is assumed that the temperature at the surfaces of the wall, buoyancy-driven fluid flow, and the glass are uniform throughout its length [40]. This assumption is justified because of the scope of the current work, which includes a global energy balance model for the easiness in the generation of the optimization results as compared to the approach based upon computational fluid dynamics. It is also assumed that the inner glass and wall surfaces are relatively smooth and the resistance to the flow owing to the friction of these surfaces can be negligible. It is also assumed that the radiation heat gain and losses are only significant for the glass cover, and the radiation heat gain and losses are ignored for windows and the roof.

For the glass cover, one of the input energy terms is the solar radiation heat flux absorbed by the glass cover S_1. Along with this, the input heat terms are the radiative heat gained by the adjacent wall $(h_{r,w-g}(T_w - T_g))$and the convective heat gains from the adjacent working fluid (air) $(h_{c,f-g}(T_f - T_g))$. Heat loss occurs from the glass of the solar chimney in terms of convective and radiative heat loss $(U_t(T_g - T_a))$. The balance can be written as (see node T_g of Fig. 1b):

$$S_1 + h_{r,w-g}(T_w - T_g) + h_{c,f-g}(T_f - T_g) = U_t(T_g - T_a) \tag{1}$$

For the fluid (air) flowing between the glass and the wall, the inlet energy term is the convective heat gain from the adjacent wall $(h_{c,w-f}(T_w - T_f))$, and the outlet terms are the convective heat loss from the fluid to the glass $(h_{c,f-g}(T_f - T_g))$and the incoming flux heat from the room $(\dot{q}'')$. It can be written as (see node T_f of Fig. 1b):

$$h_{c,w-f}(T_w - T_f) = h_{c,f-g}(T_f - T_g) + \dot{q}'' \tag{2}$$

For the wall, the input energy term is the solar radiation (transmitted by the glass cover) (S_2). The output terms are the following: convective heat loss from the wall to the adjacent air channel $(h_{c,w-f}(T_w - T_f))$, radiative loss from the wall to the glass $(h_{r,w-g}(T_w - T_g))$, and heat loss from the wall to the interior of the room $(U_{t,w-r}(T_w - T_r))$. It is given by (see node T_w of Fig. 1b):

$$S_2 = h_{c,w-f}(T_w - T_f) + h_{r,w-g}(T_w - T_g) + U_{t,w-r}(T_w - T_r) \tag{3}$$

The whole energy balance on the building-integrated solar chimney with a node at the center of the building would yield the **room air temperature**. This balance is considered based upon the lumped model without considering the temperature distribution within different space steps of the building. The infiltration and exfiltration of the air through leaks, cracks, windows, and doors is considered negligible compared to the ventilation airflow impulsed by the solar chimney. The input terms of this balance include the (a) flow heat entering the building through the inlet vent of the building to provide the mass flow to the solar chimney $\dot{m}c_p(T_a)$, (b) heat transmission through the building envelope, and the (c) interior heat generation owing to equipment and/or occupants $(\dot{q}_{gen})$. The outlet term of this balance is the flow of heat leaving the building through the outlet vent of the solar chimney $(\dot{m}c_p(T_{f,out}))$. The heat transmission through the building envelope can consist of the heat transmission through the left wall, right wall, roof, floor, front wall, back wall, one door, eight main windows, and two ventilation windows depending upon their characteristics. Nevertheless, the heat transmission from the left wall can have 'somewhat' complications because it has an integrated solar chimney. Thus, two heat transmissions must be considered for the left wall for the location where the solar chimney is attached, and for the location where it is not attached. The difference is written in terms of an area correction factor$(A_{t,frontwall} - (2 \times A_{window}) - A_{door})$ (including the window on the left wall too). The front side wall has the main door and two windows attached to it and it is multiplied with its correction factor$(A_{t,frontwall} - (2 \times A_{window}) - A_{door})$. In general, the balance can be written as (see node T_r of Fig. 1b):

More details on the explanation of the terms of equations (1)–(4) are displayed in Table A. I. Apart from this, some important sections related to the research method are displayed in Appendix A.

2.2. Performance indicators

See Table 1.

2.3. Digital twin modeling using multivariate regression and artificial neural network

Surrogate, digital twin, or metamodels are gaining popularity in recent years, especially in energy and buildings. Their necessity is that the usage of the physical or mathematical model has become very complex because of complex building physics, constraints, design procedures, and iterative solutions. Thus, it becomes computationally costly to use the iterative physical model directly for optimization purposes. Therefore, the digital twin model is preferred because it is based upon the "black box model" without involving any iterative loops and directly relates to the input vector with the output vector. In addition, the digital twin model requires a database which is called "numerical experiments". These numerical experiments are generated directly from the usage of the validated physical model over a particular range of the variables. The minimum values of L, W, d, T, I_T and v_{wind} are 0.50 m, 0.16 m, 0.05 m, 278.16 K, 400, $W/m^2$and 0.02 m/s, whereas their maximum values are 6 m, 3.5 m, 0.4 m, 323.16 m, 1000 W/m^2, and 5 m/s, respectively. Corresponding to this, the minimum value of ACH, η, and Ψ are 0.20 1/h, 6%, and 121.4 $kg_{CO_2}/m^3/year$, and their maximum values are 5 1/h, 52.8%, and 3006.7 $kg_{CO_2}/m^3/year$, respectively. More details of the adapted digital twin model can be seen in Appendix A.

2.4. Design formulation of multiobjective optimization

See Table 2.

2.5. Multicriteria decision-analysis method using the Technique for Order of Preference by similarity to ideal solution (TOPSIS)

By using multiobjective optimization techniques, especially NSGA-II, the obtained results give a couple of optimal non-dominating points on the Pareto front. This helps the decision-maker to choose the most appropriate optimal design point. For this purpose, it is required to apply a post-processing algorithm for the multicriteria decision analysis to find the final optimal solution. One of the multicriteria decision-making tools is Technique for Order Performance by Similarity to Ideal Solution (TOPSIS). The idea behind this algorithm is to choose the final optimal solution which should have the shortest geometric distance i.e., Euclidian distance from the ideal solution, and maximum longest geometric distance from the non-ideal solution. In other words, TOPSIS is a compensatory method that provides a trade-off between the user's criteria, and generally, the poor results in one of the criteria can be negated by a better result in the other criteria. The stepwise description is presented in Table 2.

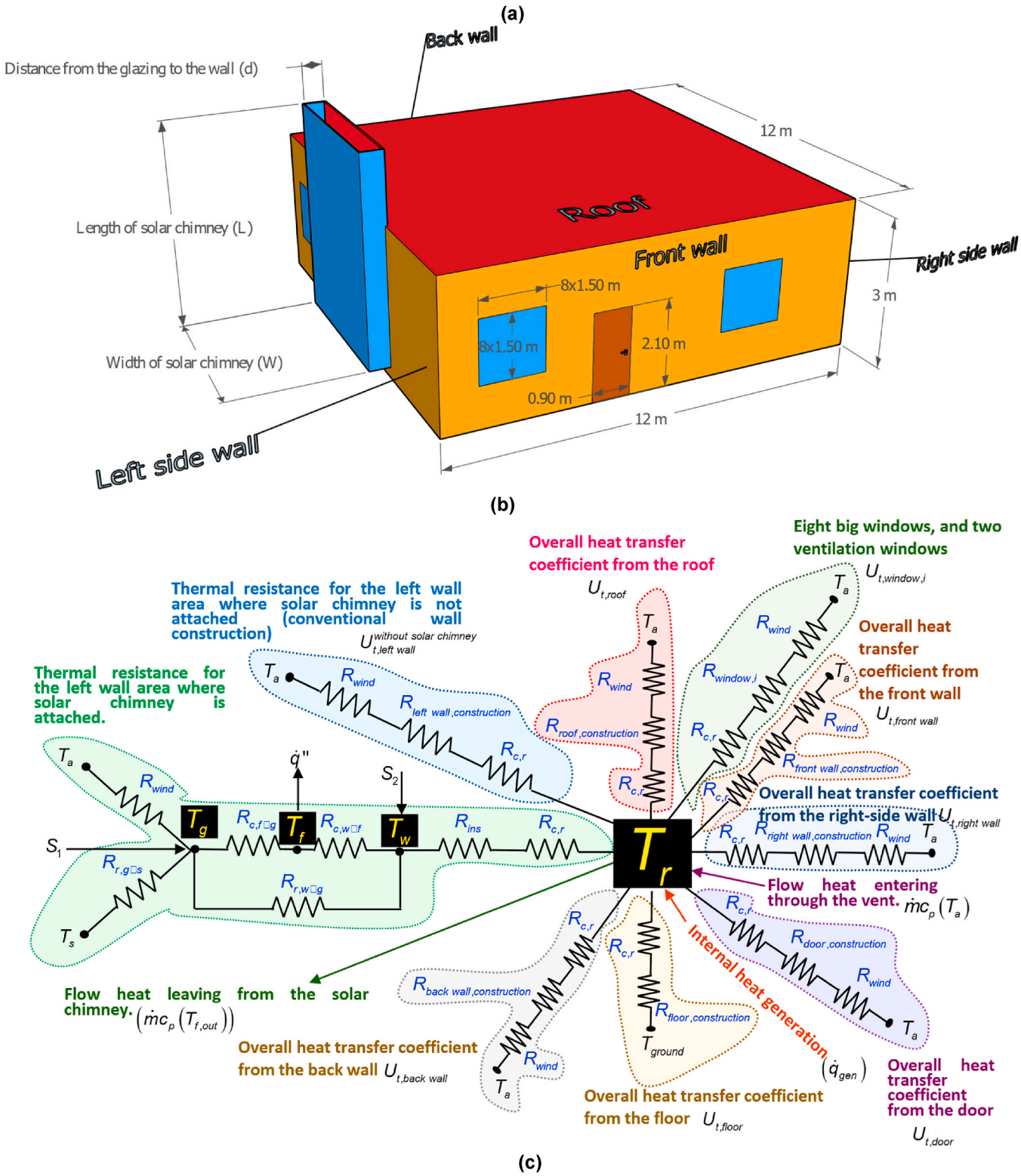

- $R_{x,construction} = \dfrac{1}{U_{x,construction}}$ (wall,window,floor,roof,door)
- $R_{c,r} = \dfrac{1}{h_r}$
- $R_{ins} = \dfrac{\Delta w_{ins}}{k_{ins}}$
- $R_{c,f-g} = \dfrac{1}{h_{c,f-g}}$
- $R_{c,w-f} = \dfrac{1}{h_{c,w-f}}$
- $R_{r,w-g} = \dfrac{1}{h_{r,w-g}}$
- $R_{wind} = \dfrac{1}{h_{wind}}$
- $R_{r,g-s} = \dfrac{1}{h_{r,g-s}}$

Fig. 1. (a) The architecture of the experimental building. (b) Thermal resistance diagram of a building-integrated solar chimney. (c) Formulas of thermal resistances which are mentioned in Fig. 1(a).

$$\overbrace{\dot{m}c_p\left(T_a\right)}^{\text{Flow heat entering the building through inlet vent of building}} + \overbrace{\left(\begin{array}{l}
\boxed{\text{Left wall}}\ \overbrace{U_{t,w-r}\left(A_{solar\ chimney}\right)\left(T_w - T_r\right)}^{\text{Heat transmission through left wall where solar chimney is attached}} + U_{t,left\ window}A_{window}\left(T_a - T_r\right) \\
\quad + \overbrace{U_{t,left\ wall}^{without\ solar\ chimney}\left(A_{t,left\ wall} - A_{solar\ chimney} - A_{window}\right)\left(T_a - T_r\right)}^{\text{Heat transmission through left wall where solar chimney is not attached}} \\
\boxed{\text{Front wall}} + U_{t,front\ wall}\left(A_{t,front\ wall} - \left(2\times A_{window}\right) - A_{door}\right)\left(T_a - T_r\right) \\
\quad + U_{t,door}A_{door}\left(T_a - T_r\right) + U_{t,front\ window}\left(2\times A_{window}\right)\left(T_a - T_r\right) \\
\boxed{\text{Right side wall}} + U_{t,right\ wall}\left(A_{t,right\ wall} - \left(3\times A_{window}\right)\right)\left(T_a - T_r\right) + U_{t,right\ window}\left(3\times A_{window}\right)\left(T_a - T_r\right) \\
\boxed{\text{Back side wall}} + U_{t,back\ wall}\left(A_{t,back\ wall} - \left(2\times A_{window}\right) - \left(2\times A_{ventilation,window}\right)\right)\left(T_a - T_r\right) \\
\quad + U_{t,back\ window}\left(2\times A_{window}\right)\left(T_a - T_r\right) + U_{t,back\ ventilation,window}\left(2\times A_{ventilation,window}\right)\left(T_a - T_r\right) \\
\boxed{Roof} + U_{t,roof}A_{t,roof}\left(T_a - T_r\right) \qquad \boxed{Floor} + U_{t,floor}A_{t,floor}\left(T_{ground} - T_r\right)
\end{array}\right)}^{\text{Heat transmission through building envelope}} + \overbrace{\dot{q}_{gen}}^{\text{Internal heat generation}} = \overbrace{\dot{m}c_p\left(T_{f,out}\right)}^{\text{Flow heat leaving the building through outlet vent to the solar chimney}} \tag{4}$$

Table 1
Description of the performance indicators.

Performance indicator	Description
Air changes per hour (ACH)	One of the prime functions of a solar chimney is to provide an adequate ventilation rate ($\dot{V}_o$) within the building without using any turbomachinery. ANSI/ASHRAE standard 62.1 [41] has recommended a minimum of 5 CFM (≈8.5 m^3/h) per person for a dwelling unit in a residential type of building valid for ETS-free zone, and by considering default occupancy density. It is desired to maximize the ventilation rate ($\dot{V}_o$). One alternative of the ventilation rate ($\dot{V}_o$) is to express it in **"air changes per hour** (ACH)**"** which is calculated by taking a ratio of the ventilation rate with respect to the volume of the building. Like the ventilation rate ($\dot{V}_o$), it is also desired to have the maximum value of the number of air changes (ACH) to take away the pollutants of the indoor built environment, along with an aim to supply the fresh air to the occupants. It is defined by: $ACH = \frac{\dot{V}_o}{\text{Volume of the building}}$ where $\dot{V}_o = 3600 \times C_d \frac{A_o}{\sqrt{1+A_r}}\sqrt{\frac{2gL\left(T_f - T_r\right)}{T_r}}$ (5) $\dot{V}_o$ is multiplied by 3600 s to yield the units the ventilation rate ($\dot{V}_o$) in m^3/h, and finally, the units of ACH are in 1/h (air change per hour).
Energy efficiency (η)	The **energy efficiency** (η) of the solar chimney is a performance indicator that indicates the degree of the exploitation of the incoming solar energy (WLI_T) in the form of the heat collection of the solar chimney ($\dot{m}c_f(T_{f,o} - T_{f,i})$). It is desired to maximize the energy efficiency and it can be written as: $\eta = \frac{\dot{m}c_f\left(T_{f,o} - T_{f,i}\right)}{WLI_T}$ (6)
Specific environmental influence (Ψ)	With the context of the global warming issues, the third performance indicator is related to the environmental degradation resulting from the usage of the solar chimney as compared to the shaft-driven fan. For this purpose, it is desired to estimate the equivalent fan shaft power which compensates for the usage of a ventilation fan. The equivalent shaft power (ϖ) considering a static pressure (P_s) of 1000 Pa [42], and a fan efficiency (η_{fan}) of 70% [42], can be written as: $\varpi = \frac{P_s\dot{V}_o}{\eta_{fan}} \times \frac{1000}{3600}$ (7) Eq. (7) is multiplied by the factor $\frac{1000}{3600}$ to convert the units of equivalent shaft power into kW considering the units $\dot{V}_o$ to be in m^3/h. The **specific environmental influence** (Ψ) of the usage of the solar chimney can be known by multiplying the emission factor of the electricity usage ($EF_{electricity}$) with the equivalent shaft power (ϖ) with respect to the total volume of the building. It is given by: $\Psi = \frac{(\varpi \times 8760) \times EF_{electricity}}{\text{Volume of the building}}$ (8) The emission factor of the electricity usage ($EF_{electricity}$) considers the embodied energy and CO_2 emissions of an electricity grid used to supply the electricity to the equivalent shaft power of the fan. It consists of various life-cycle stages, including raw material extraction, equipment manufacturing, energy production, distribution, usage, and disposal. A global average emission factor of electricity is 0.623 kg_{CO2e}/kWh [43]. Eq. (8) is divided by the volume of the building to remove the subjectivity of the building size and extend its interpretation. Finally, it is multiplied with the 8760 h to convert the units of the specific environmental influence (Ψ) into kg_{CO2e}/m^3 for a one-year duration.

3. Results and discussion

3.1. Digital twin using the multivariate regression method

The multivariate regression method is applied to the statistical package called STATGRAPHICS [49]. The results are supported with a MANOVA (**M**ultivariate **AN**alysis **O**f **VA**riance), estimation of parameters, and the satisfaction of the assumptions of this technique which are displayed in Table B.I (Appendix B) and Fig. 2.

The objective of MANOVA is to provide the details of the source of the variation, and the statistical significance of the model and the input variables. The term "source" refers to the source of variation which can be a result because of the variation of the "model" or because of the variation within its "residue". The total variation is explained by the total sum of squares which is the summation of the sum of squares from the model (explained variation), and the sum of squares from the residue (unexplained variation). The model variation is due to the interaction between the samples for the Sum of Squares Between groups. The

Table 2
Stepwise description of (a) multiobjective optimization problem formulation, and (b) TOPSIS technique.

(a) Stepwise description of the design formulation involved in the multiobjective optimization study.

Optimization step	Details
Objective functions	The objective functions are the three performance indicators which are air changes per hour(ACH), energy efficiency(η), and specific environmental influence (Ψ)
Design variables, search space, and design constraints	Several design variables are ranging from geometric, operational, flow, and climatic characteristics. The key geometric variables in the vertically installed solar chimney are the height (length of the solar chimney in the upward vertical flow direction) (L), width (horizontal dimension or the amplitude) (W), and the spacing between the glass cover and the wall(d). The weather data conditions including the ambient temperature (T_a), solar radiation(I_T), and wind velocity (v_{wind}) are also taken as design variables which are selected depending upon the subject location.
Optimization problem	In summary, the multiobjective optimization aims to maximize the air changes per hour (ACH) and energy efficiency(η)and minimize the specific environmental influence (Ψ) while looking between the search space of the length, width, and the spacing between the glass cover and the wall. The optimization also has restrictions related to the ambient temperature, solar radiation, and wind velocity which are subjected to the weather conditions. Mathematically, it can be written as: Objective function: $\min f = \begin{cases} f_1 : -ACH \\ f_2 : -\eta \\ f_3 : \Psi \end{cases}$ Search space: $0.5m \leq L(\text{length of the solar chimney}) \leq 6m$ $0.1m \leq W(\text{width of the solar chimney}) \leq 3.5$ $0.05m \leq d(\text{spacing between the glass cover and the wall}) \leq 0.4m$ Restrictions: $T_a, I_T,$ and v_{wind} which depends upon the weather conditions (see Table A.II)
Theory of optimization algorithm	A genetic algorithm (GA) is used for optimization purposes which is a metaheuristic algorithm that has an analogy with the natural evolution "survival of the fittest" from Charles Darwin's theory. There are many steps to mimic the GA to find the optimization solution. In preprocessing, each variable is converted into a binary number with a certain number of bits. After the preprocessing, many steps are taken to reach the global optimal. In the first step, an initial population is created in which each member is considered as a string with a specific bit size. The initial size of the population is a tuning parameter that can be experimented with. In the second step, an evaluation process is carried out in which the value of the variables for each member is extracted and the function values are evaluated, known as "fitness values". In the third step, the reproduction process takes place which has further three sub-steps, (a) mating pool, (b) crossover operation, and (c) mutation. For reproduction, it is desired to create a (a) mating pool of individuals. The mating pool can be created randomly but using a roulette wheel is also common which is used to make the copies of the fittest members for reproduction. The simulated roulette wheel selection provides a proportional chance of a member being selected to its scale of fitness value. In the next sub-step of the reproduction process, (b) a crossover operation is performed on the mating parent pool to produce offspring. It is made possible by replacing a certain quantity of the binary digits of the individuals in the same mating pool which is guided by a user-defined probability of crossover operation. In the third sub-step of the reproduction, (c) mutation process is applied after the selection i.e., mating pool, and crossover operation. It is made possible by replacing (0 by 1, or 1 by 0) a certain percentage of the binary code of the individuals which is controlled by a mutation percentage. In the last step, a reevaluation takes place which evaluates the fitness value of the new individuals and compares them with the previous generation. The algorithm retains the individuals with the "survival fit" and discards other individuals [44]. The presence of multiple objectives "multiobjective optimization" in the problem raises a set of non-dominating optimal solutions which is represented on a Pareto front. This is not true for single-objective optimization where the optimality is a unique point. One variation called a nondominated sorting genetic algorithm (NSGA) is robust to handle such multiobjective optimization problems. It uses a ranking selection method to emphasize good points and a niche method is used to maintain stable subpopulations of good points. The only variation bought by NSGA is related to the operation of the selection procedure, whereas the crossover and the mutation processes are the same. In NSGA, the population is ranked based on a nondomination of an individual before the selection is performed on the individuals. This helps NSGA to maintain stable and uniform reproductive potential across nondominated individuals. Baluja et al. [45] have commented that the usage of elitist selection can monotonically increase the quality of the best solution in each generation i.e., elitism is a general process of constructing a new population while allowing the best individuals from the current generation to be moved unaltered to the next generation. NSGA is generally criticized because it has a high computational complexity of non-dominating sorting and can be expensive for large population sizes. Thus, there are also various variations to improve the performance of NSGA, especially the one proposed by Deb et al. [46] which includes the elitism trait (apart from two more difficulties, computational complexity, and the need for specifying a sharing parameter). The modified version, called NSGA-II, involved two more variables, called rank, and crowding distance. An elitist GA (NSGA-II) always favors the individuals with better fitness values which is defined as rank. In such an iterative definition, it is proposed that rank k individuals are dominated only by individuals in rank k-1 or lower. The crowing distance is a measure of the closeness of an individual to its nearest neighbors. NSGA-II measures the distance among individuals of the same rank. This helps to identify the real neighborhood of an individual and the crowding distance also aids to identify the rank of the individuals. In this way, individuals of the same rank with a higher distance have a higher chance of selection. Crowding distance also helps to select between the individuals having the same rank. The stopping criteria of the algorithm are determined by the spread which is a measure of the movement of the Pareto set. The algorithm calculates the standard deviation of the crowding distance measure of points that are on the Pareto front with finite distance. The algorithm also calculates the sum over the objective function indices of the norm of the difference between the current minimum-value Pareto point for that index and the minimum point for that index in the previous iteration. The extreme objective function values do not change much between the iterations when the spread is small. This is also used as stopping criteria and the iterations halt when the spread does not change much [47].
Implementation of the optimization algorithm	Non-dominating sorting elitist genetic algorithm (NSGA-II) is implemented on MATLAB [48] using the built-in function `gamultiobj`. Several parameters which are used to support the optimization algorithm are as follows: a. Population size: 200 (more than five variables) b. Selection function: Tournament c. Crossover fraction: 0.8 d. Migration: Forward direction e. Migration fraction: 0.2 f. Distance measuring function: Crowd distancing g. Pareto front population fraction: 0.32 h. Hybrid function: None i. Stopping criteria (generations): 100 x (number of variables) j. Stopping criteria (time limit): Infinite

(*continued on next page*)

Table 2 (*continued*)

(a) Stepwise description of the design formulation involved in the multiobjective optimization study.

Optimization step	Details
	k. Stopping criteria (fitness limit): Infinite l. Stopping criteria (function tolerance): 1e-4 m. Stopping criteria (constraint tolerance): 1e-3

(b) Stepwise description and implementation of multicriteria decision-analysis method applied on Pareto front.

Steps	Details
Step 1: Normalization	Normalization is required because the three performance criteria have a non-homogenous range of operation. It is done by creating non-dimensional vectors of the solution determined by the Euclidian non-dimensioning method, given by: $$f_{normalized} = \frac{f_i}{\sqrt{\sum_{i=1}^{num_i} [f_{ij}]^2}} \quad (9)$$ Here, $f_{normalized}$ represents the vector of the normalized objective functions. The term f_i is the vector of the objective functions. The term $\sqrt{\sum_{i=1}^{num_i} [f_{ij}]^2}$ represents the Euclidian norm which is calculated using the default built-in function of MATLAB called `norm`.
Step 2: Ideal and non-ideal solutions	The ideal and non-ideal hypothetical solution points are calculated. For example, the ideal point ($f_{normalized,j}^{idealpoint}$) on the Pareto front for this multiobjective optimization is the maximum "air changes per hour (ACH)", maximum energy efficiency (η), and minimum specific environmental influence (Ψ). Similarly, the non-ideal point ($f_{normalized,j}^{non-idealpoint}$) is minimum "air changes per hour (ACH)", minimum energy efficiency (η), and maximum specific environmental influence (Ψ). The ideal and non-ideal points are necessary to find the relative distance of each optimal point with respect to these points.
Step 3: Positive and negative Euclidian distance	Using the ideal and non-ideal points, the positive (d_i^+) and negative Euclidian distance (d_i^-) is calculated with respect to each optimal point. It is given by: $$d_i^+ = \sqrt{\sum_{j=1}^{num_{obj}} \left[f_{normalized} - f_{normalized,j}^{idealpoint}\right]^2} \; d_i^- = \sqrt{\sum_{j=1}^{num_{obj}} \left[f_{normalized} - f_{normalized,j}^{non-idealpoint}\right]^2} \quad (10)$$
Step 4: Relative closeness	The relative closeness (RC_i) of each alternative with respect to the ideal (d_i^+) and non-ideal (d_i^-) distance is calculated using: $$RC_i = \frac{d_i^+}{d_i^- + d_i^+} \quad (11)$$
Step 5: Sorting	The matrix (RC_i) is sorted and the values of objective functions and decision variables with the maximum value of (RC_i) is the final selected optimal point.

residue variation refers to the variation due to the differences within the individual samples. The degrees of freedom refer to the number of values that are free to vary in a dataset. The degree of freedom of the model is 27 which represents six basic design variables $L, W, d, T_a, I_T, v_{wind}$, 6-s order terms $L^2, W^2, d^2, T_a^2, I_T^2, v_{wind}^2$, and fifteen interactions within the six design variables $L \times W, L \times d, L \times T, L \times I_T, L \times v_{wind}, W \times d, W \times T_a, W \times I_T, W \times v_{wind}, d \times T_a, d \times I_T, d \times v_{wind}, d \times I_T, T_a \times v_{wind}, I_T \times v_{wind}$. In this way, the allowable degree of freedom for the residue "data" would be the total data size minus the 27 variables of the model i.e., 1079 (Table B.I (a)). The mean square is calculated by dividing the sum of squares with the degree of freedom i.e., $4101.72/27 = 151.916$ (Table B.I (a)). The mean square is analogous to the variance of a distribution. In this way, a higher mean square value would correspond to a higher variance in the data.

One of the prime objectives of ANOVA is to evaluate the ratio between the mean square of the model and the mean square of the residue. Such a ratio, called F-ratio would provide the information that how many times greater the variance due to the model is than the variance due to the uncontrolled effects. In other words, F (Fisher) ratio determines the variation between the sample with respect to the variation within the sample i.e., in Table B.I (a), the F ratio is 5794.97 which is obtained by dividing 151.916 by 0.0262151. It signifies that the between groups (model) variance is 5794.97 times the size of the within-group variance (residue). The F-value answers the question of there exists an overall significant regression model for the subject problem. The null hypothesis states that the regression model is significant, and the alternate hypothesis states that the regression model is not significant. In other words, the null hypothesis is a test of lack of fit which is $H_0 : Y_i = C^o + \sum_{i=1}^{n} C_i^1 X_i + \sum_{i=1}^{n} \sum_{j=1}^{n} C_{ij} X_i X_j + \ldots + \sum_{i=1}^{n} \sum_{j=1}^{n} \ldots \sum_{q=1}^{n} C_{ij} \ldots \underbrace{[X_i X_j \ldots X_n]}_{\text{terms of max power}} + e_i$ and the alternate hypothesis is $H_1 : Y_i \neq C^o + \sum_{i=1}^{n} C_i^1 X_i + \sum_{i=1}^{n} \sum_{j=1}^{n} C_{ij} X_i X_j + \ldots + \sum_{i=1}^{n} \sum_{j=1}^{n} \ldots \sum_{q=1}^{n} C_{ij} \ldots \underbrace{[X_i X_j \ldots X_n]}_{\text{terms of max power}} + e_i$. Thus, it is necessary to calculate the critical F value to test the hypothesis. The critical F value calculated using 27 degree of freedom in the numerator and 1079 degree of freedom in the denominator with a 95% confidence interval corresponding to an alpha value of 0.05 gives 1.50 (calculated using an interactive table of reference [50]). It signifies that the calculated F-value is higher than the critical F-value (Table B.I (a)), indicating that the null hypothesis is rejected which apparently informs that the regression model is not significant. In other words, the lack of fit of the adjusted regression is significant. However, taking this decision without considering the p-value is not helpful because the F-statistic must be used in combination with the p test to decide the significance of the overall results. The null hypothesis of the p-value is $H_0 : C^o = C_i^1 = C_{ij} = 0$ and the alternate hypothesis is $H_1 : \text{At least one } C \neq 0$. The null hypothesis states that the coefficients of the design variables do not explain the goodness of fit of the predicted indicator. The alternate hypothesis states that the goodness of fit of the predicted indicator is explained by at least one of the design variables. In other words, the alternate hypothesis states that at least one of the design variables is not zero. Here (Table B.I (a)), it can be seen that the p-value is 0 which is less than the critical significance level of 0.05 considering a confidence interval of 95%. In other words, lower probabilities (p-values) are indicators of goodness of fit. Thus, the null hypothesis can be rejected which interprets that the regression model is significant. In other words, the hypothesis test signifies that at least one of the design variables in the estimation of the performance indicator exists which is not zero. Putting the explanation, in summary, the F-statistics just compares the joint effect of all the variables together, and it is recommended to consider the p-test too. Revising Table B.I (a, b, and c), it can be concluded that the regression models of air changes per hour ACH, energy efficiency (η), and specific

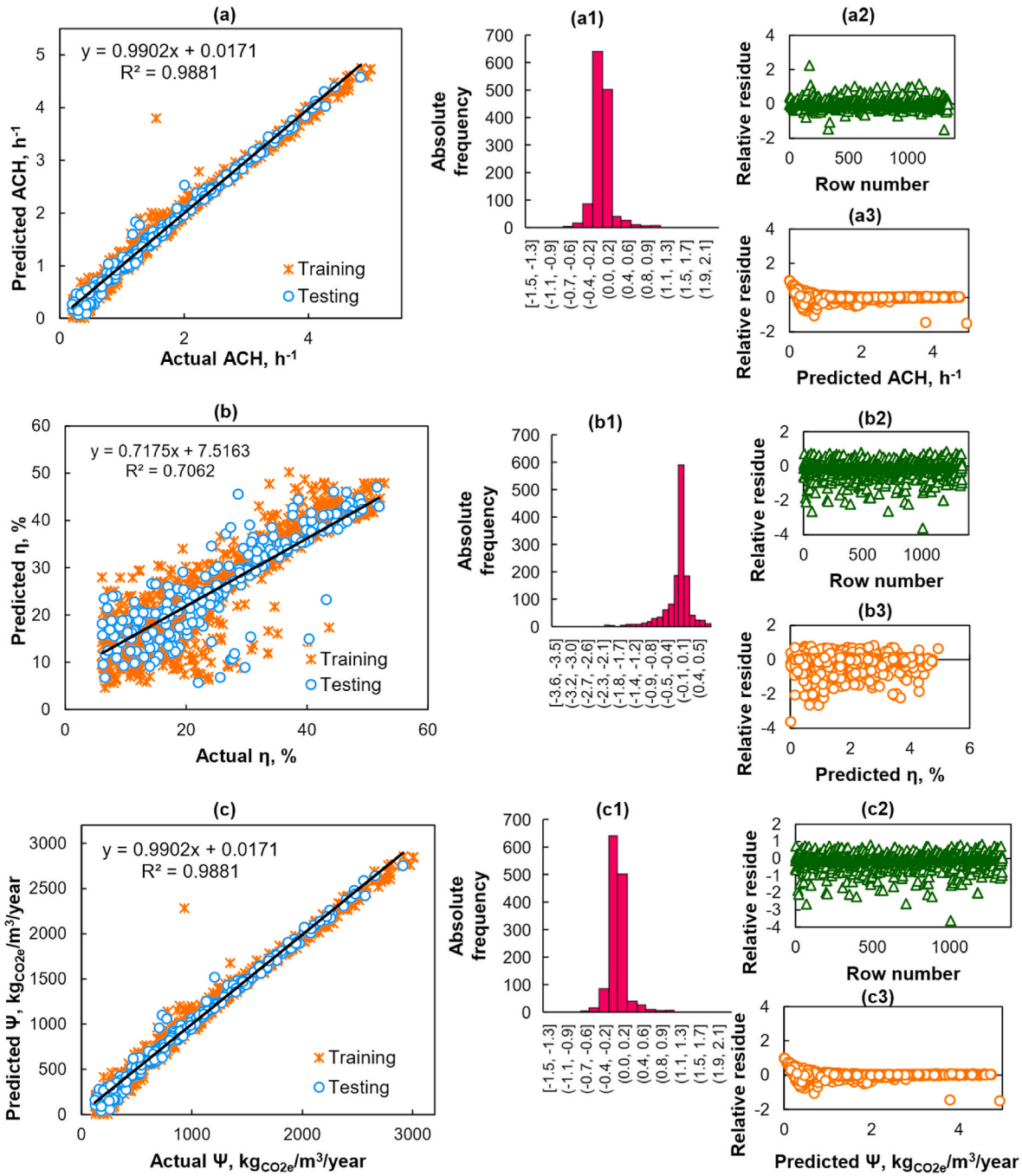

Fig. 2. Regression fit of the application of multivariate regression method on **(a)** air changes per hour (*ACH*), **(b)** energy efficiency (η), and **(c)** specific environmental influence (Ψ). **(a1, b1, and c1)** displays the normality assumption of errors. **(a2, b2, and c2)** displays the independence assumption of errors. **(a3, b3, and c3)** displays the homoscedasticity assumption of errors.

environmental influence (Ψ) are statistically significant with a confidence interval of 95%.

Even though it is proved that the regression models are significant, but it does not provide the information that if each one of the parameters (including linear design variables, higher-order design variables, and their interactions) can contribute significantly to their respective model. This information is displayed in Table B.I (a1, b1, and c1). These tables contain the parameter in the first column and the estimated value of the coefficient of the respective parameter. These estimations are actually the weight coefficients of each of the parameters. For example, the multivariate regression equation of air changes per hour (*ACH*) can be written as follows using the estimation weight coefficients of Table B.I (a1):

$$ACH = -0.215852L - 0.567914W - 3.94004d + 0.0053464T_a - 0.0258362L^2 - 5.13382d^2 - (5.56726E-7)I_T^2 + 0.179655(L \times W) + 1.16865(L \times d) + 0.000147119(W \times I_T) + 0.00240612(d \times I_T) \quad (12)$$

It is pertinent to mention that each significant value of each coefficient is important to yield the correct predicted value *ACH*. The next column is related to the standard error in the estimation coefficient which is also an estimator of the standard deviation in the estimated coefficient. Its interval can be calculated using (Estimation $\pm$ $z_{\alpha/2}$ $\times$ Standard error). The next column shows the details of the (student's) T statistic which is calculated by dividing the estimation coefficient by the

standard error. For example, in Table B.I (a1), the T statistic is −2.59469 which is obtained by dividing −0.215852 with 0.0831898. The second last comment shows the p-value of each parameter. A p-value less than 0.05 indicates a statistical significance of the relative parameter for a confidence interval of 95%. If the p-value is greater than 0.05, then, the parameter is not statistically significant. In other words, a p-value equal to or higher than 0.05 indicates that the relative parameter does not contribute in any way towards the lack of fit of the performance indicator. Thus, the parameters having non-significance statistically can be left out while writing the final equation. Note, eq. (12) does not contain I_T, v_{wind}, W^2, T_a^2, v_{wind}^2, $L \times T$, $L \times v_{wind}$, $W \times T_a$, $W \times v_{wind}$, $d \times T_a$, $d \times v_{wind}$, $T_a \times v_{wind}$ and $I_T \times v_{wind}$ because they were statistically insignificant.

It should be noted that v_{wind} does not appear in eq. (12). Physically, it might not be correct because the wind velocity can change the convective heat transfer coefficient of the glass to the environment, leading to different glass temperatures which would finally influence the volume flow rate and the number of air changes (ACH). The absence of v_{wind} in eq. (12) merely reflects the behavior of the utilized data and the property of the regression method which seems to have a high value of the coefficient of determination even when v_{wind} is excluded.

Fig. 2 (a, b, and c) shows the wider perspective of the overall performance of the multivariate regression method. It can be seen that the total data is also divided into two parts, namely, training and testing data with 85% and 15% of distribution, respectively. The training data is used to develop the multivariate regression model, and the remaining 15% is used to test the performance of the regression model. It can be seen that both datasets are in harmony with an R^2 value of 0.981, 0.7062, 0.9881 for air changes per hour (ACH), energy efficiency (η), and specific environmental influence (Ψ), respectively. Even though the coefficient of determination is acceptable for common statistical application, nevertheless, the coefficient of determination for energy efficiency is too low to be used as a reliable surrogate of the physical model.

Another perspective of the multivariate regression is shown in Fig. 2 (a1, a2, a3, b1, b2, b3, c1, c2, and c3). There are three main assumptions on the behavior of the errors or residuals of the regression fit. It is characterized by a relative residual which is calculated by placing a difference between the actual value of the performance indicator and the predicted value of the performance indicator and all together divided by the actual value of the performance indicator. The three assumptions are (a) normality, (b) independence, and (c) homoscedasticity, of errors. If the normality of errors is not met, then the confidence interval may become too wide or narrow, bringing instability in the confidence interval. This leads to the difficulty in estimating coefficients based on the least square method. It is verified by plotting a normal bell curve distribution of the relative residual as shown in Fig. 2 (a1, b1, and c1). The independence of the error signifies that the error terms are uncorrelated, and the error terms are independent random variables. It is verified by plotting the relative residual with respect to the row number as shown in Fig. 2 (a2, b2, and c3). The objective is to attain a graph with no definite patterns. The third assumption is that there should be a constant variance in the error terms and this phenomenon is called homoscedasticity. It is diagnosed by plotting the relative residual with the predicted performance indicator and the idea is not to obtain any definite patterns in this graph.

It can be noted that all the performance indicators comply with the two assumptions of the regression fit (independence and homoscedasticity). However, it seems like that the bell curve is too elongated in the upwards direction which can yield a kurtosis greater than zero and deviate from the normal distribution curve.

3.2. Digital twin using multilayer perceptron artificial neural network and sensitivity analysis

MLP-ANN model is implemented on the neural net fitting tool `nftool` [51] on the interface of MATLAB [48]. The total database of 1584 vectors (6 input points and three output points) are divided into 70%, 15%, and 15% for training, testing, and validation purpose. The number of hidden layers is varied from 1 to 10 to determine the optimal architecture for each of the performance indicators. The optimal architecture for air changes per hour (ACH) is 6-8-1 where 6 represents the number of input variables, 8 represents the number of hidden layers, and 1 represents the output variable (ACH). The optimal architecture for energy efficiency (η) and specific environmental influence (Ψ) is 6-10-1 and 6-9-1, respectively. Iterations are also carried out on three different backpropagation algorithms namely are Levenberg–Marquardt, Bayesian Regularization, and Scaled Conjugate Gradient. It is reported that the LM backpropagation algorithm was optimal in all the architectures. The total number of iterations involving one cycle through the full training dataset, called Epoch, for air changes per hour (ACH), energy efficiency (η), and specific environmental influence (Ψ) are 87, 94, and 67, respectively.

Fig. 3 has described that the coefficient of determination of air changes per hour (ACH), energy efficiency (η), and specific environmental influence (Ψ) are 0.9881, 0.9894, and 0.9881, respectively. The curve fit performance measurement of MLP-ANN is better than the performance of the multivariate regression method especially because of the usage of non-linear adaptive machine learning algorithms used in MLP-ANN. It is also noted that the regression fit assumptions of (a) normality, (b) independence, and (c) homoscedasticity of errors are also satisfied through the usage of MLP-ANN. Thus, it can be concluded that the digital twin model using MLP-ANN is preferred for its better statistical performance and would be used for the optimization process.[2]

The conclusion of this comparison actually gives the response to the original research gap that if the regression model of Shi et al. [34] is sufficient enough. Thus, it is identified that the usage of the regression method is not ultimate in solar chimneys because it does not fulfill the regression assumptions of normality. Alternatively, it can be concluded that the digital twin model using MLP-ANN is preferred for its better statistical performance and would be used for the optimization process.

Another perspective of this discussion is related to the weights of each neuron assigned in the architecture of the MLP-ANN algorithm. It is known that the weight actually represents the significance of a variable in the model. In fact, Garson [39] has proposed an equation that provides a sensitivity analysis of the design variables on the performance indicators just using the connection weights of the neural network.[3]

The findings of the application of sensitivity analysis are displayed in Fig. 4. It is noted that the most influential variable for air changes per hour (ACH)is the distance from the glass to the wall, solar radiation, and the width of the solar chimney. Here, it makes sense that the ambient temperature is not influential because it is not the prime variable to drive the ventilation within the solar chimney. The most influential parameter for energy efficiency (η) is the distance from the glass to the wall, input solar radiation, and ambient temperature. The most influential parameter for specific environmental influence (Ψ) is width, distance from the glass to the wall, and ambient temperature. It can be

[2] The MATLAB file of digital twin model using multilayer perceptron artificial neural network is attached separately as a supplementary document.

[3] The equation is $I_j = \left[\sum_{m=1}^{m=N_h}\left[\left(\frac{|W_{jm}^{ih}|}{\sum_{k=1}^{N_i}|W_{km}^{ih}|}\right)\times |W_{mn}^{ho}|\right]\right] \div \left[\sum_{k=1}^{k=N_i}\left[\left(\sum_{m=1}^{m=N_h}\left[\left(\frac{W_{km}^{ih}}{\sum_{k=1}^{N_i}|W_{km}^{ih}|}\right)|W_{mn}^{ho}|\right]\right)\times |W_{mn}^{ho}|\right]\right]$. Here, I_j represents the relative importance of any jth input variable $(L, W, d, T_a, I_T, v_{wind})$ on one of the output variables i.e. air changes per hour (ACH), energy efficiency (η), and specific environmental influence (Ψ). N_i and N_h are the number of neurons in the input and hidden layers, respectively. The subscripts I, h and o refers to the input, hidden, and output layers, respectively. The subscripts k, m and n represents the neurons in the input, hidden, and output layers, respectively. The symbol Wrepresents the weight of the neuron.

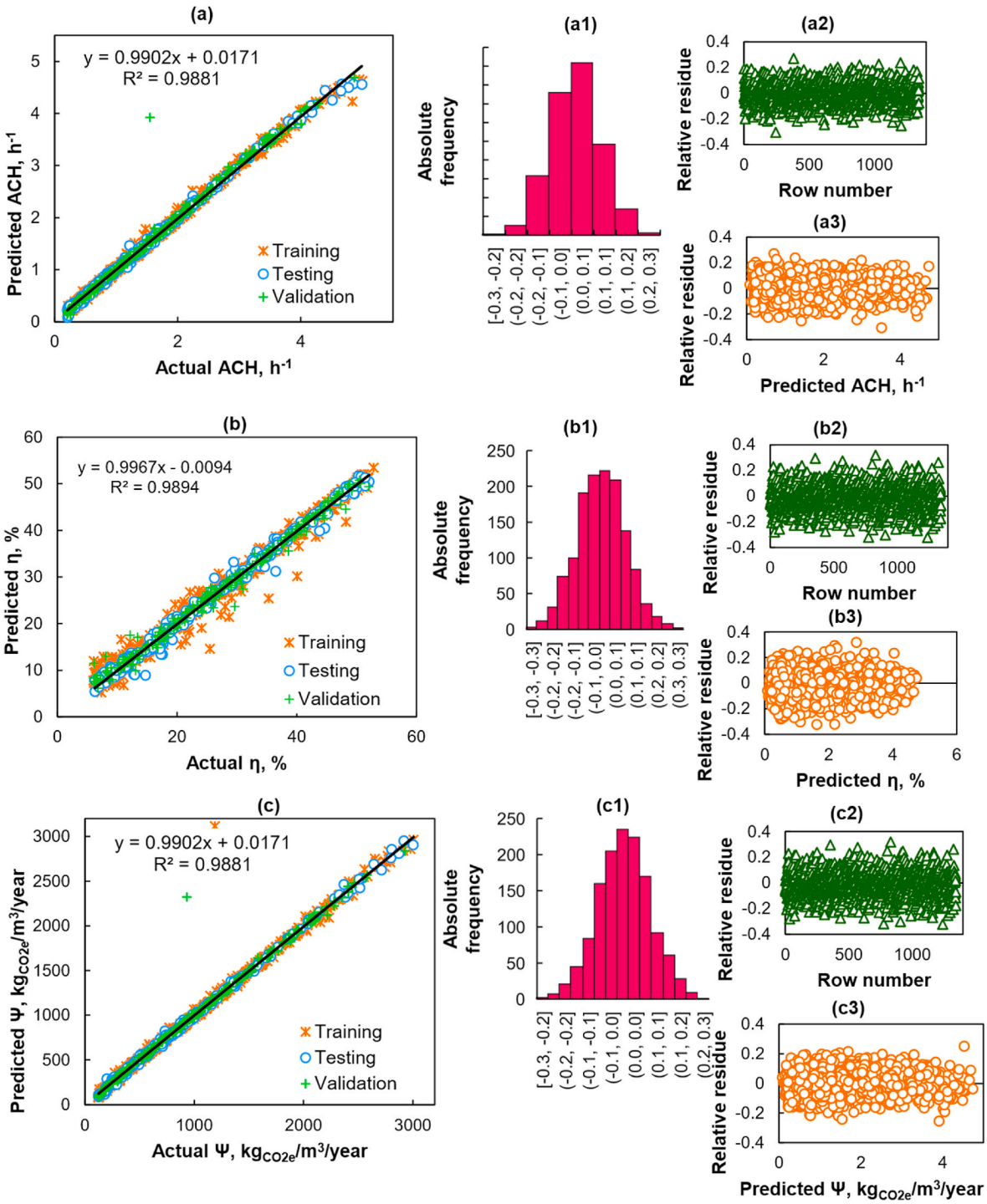

Fig. 3. Regression fit of the application of MLP-ANN technique on **(a)** air changes per hour (*ACH*), **(b)** energy efficiency (η), and **(c)** specific environmental influence (Ψ). **(a1, b1, and c1)** displays the normality assumption of errors. **(a2, b2, and c2)** displays the independence assumption of errors. **(a3, b3, and c3)** displays the homoscedasticity assumption of errors.

noted that the wind velocity is the least sensitive parameter in all cases which only changes the convective heat loss coefficient from the glass cover to the environment.

3.3. Optimization results

The optimization results after the implementation of the NSGA-II technique are displayed in Fig. 5 in the form of a Pareto front for all four climatic zones. It is also compared with a base case condition, and it is reported in Table 3.

It can be noted that for all cases, *ACH* ranges from a minimum of 0.5 1/h to a maximum of ~5 1/h, whereas this diversity of range is not noted in the efficiency especially for the tropic and dry climatic zones. The optimal region for the tropical and dry climatic zone refers to an efficiency ranging from 28% to ~34%. The environmental emissions have the highest variance in their optimal points because it is magnified too much even with the small changes in the volumetric flow rate of air in the solar chimney. Fig. 5 also shows the final selected optimal points

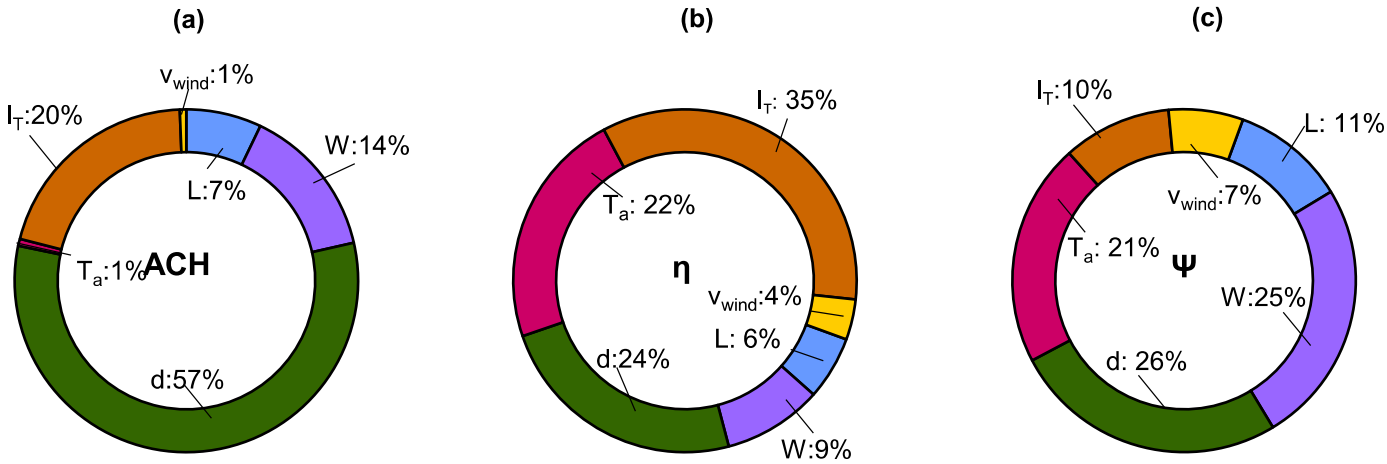

Fig. 4. Sensitivity analysis based on the Garson equation for (a) air changes per hour (*ACH*), (b) energy efficiency (η), and (c) specific environmental influence (Ψ).

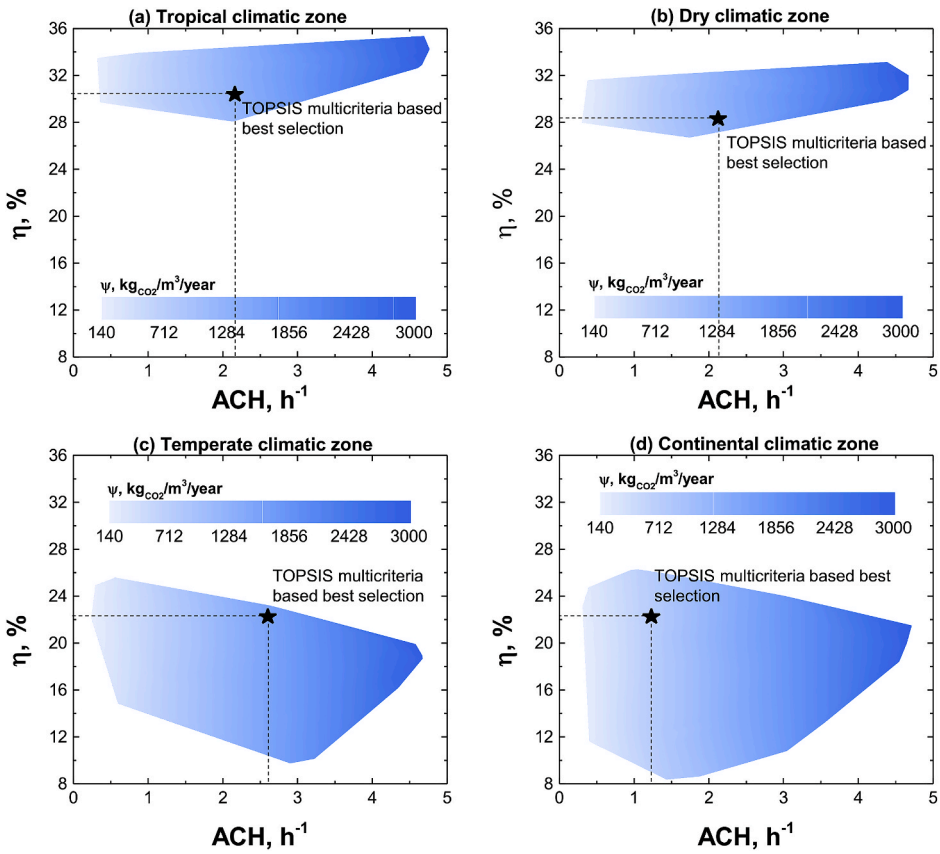

Fig. 5. NSGA-II optimization results and TOPSIS best selection displayed on the Pareto front for (a) tropical, (b) dry, (c) temperature, and (d) continental climatic zone.

through TOPSIS multicriteria selection and these points have the highest value of the relative closeness (RC_i) parameter.

In the case of temperature and continental climatic zone, the optimal points refer to an energy efficiency ranging from as below as ~8% to around 26%. It is special because of the characteristics of the temperate and continental climatic zones. In the temperate climatic zone, the solar radiation is less than the other climatic zones, decreasing the energy efficiency by only 23.18%. In the case of the continental climatic zone, the ambient temperature is relatively less than the other climates, increasing the convective and radiative heat loss coefficient from the glass to the environment. As a result of the heat loss from the solar chimney, enough thermal push is not created yielding lower values of a number of air changes per hour as compared to the other zones. Even though it is lower as compared to the other climatic zones, yet it is still higher than the minimum number of air changes recommended by the ASHRAE 62 standard.

The environmental footprints of the temperate climatic zone have resulted from a trade-off between its ventilation rate and the environmental footprints through the TOPSIS technique. It is correlated with its number of air changes which is also the highest (2.64 1/h) even though its available area to intercept the solar radiation is just 30.18 (W/m^2)/m^2 which is much less as compared to the tropical climatic zone i.e.

Table 3
Comparison of base case conditions with the optimized case conditions for **(a)** tropical, **(b)** dry, **(c)** temperate, and **(d)** continental climatic zone.

Parameter	Base case condition	Optimized case	Comments	Parameter	Base case condition	Optimized case	Comments
(a) Tropical climatic zone				**(b) Dry climatic zone**			
L, m	1.8	5.0	The base case condition is discarded because it does not satisfy ASHRAE standard 62.		1.8	6.0	The base case condition is discarded because it does not satisfy ASHRAE standard 62.
W, m	0.8	1.7		W, m	0.8	3.5	
d, m	0.145	0.3		d, m	0.145	0.05	
T_a, K	307.8	307.8		T_a, K	307.66	307.66	
$I_T, W/m^2$	695	695		$I_T, W/m^2$	753	753	
$v_{wind}, m/s$	3.61	3.61		$v_{wind}, m/s$	1.94	1.94	
$ACH, 1/h$	0.38	2.3		$ACH, 1/h$	0.39	2.13	
$\eta, \%$	–	31.3		$\eta, \%$	–	28.09	
$\Psi, kg_{CO_2}/m^3/year$	–	1379.8		$\Psi, kg_{CO_2}/m^3/year$	–	1158.1	
(c) Temperate climatic zone				**(d) Continental climatic zone**			
L, m	1.8	5	The base case condition is discarded because it does not satisfy ASHRAE standard 62.	L, m	1.8	3.5	The base case condition is discarded because it does not satisfy ASHRAE standard 62.
W, m	0.8	3.3		W, m	0.8	2.4	
d, m	0.145	0.14		d, m	0.145	0.10	
T_a, K	300.96	300.96		T_a, K	298.26	298.26	
$I_T, W/m^2$	498	498		$I_T, W/m^2$	799	799	
$v_{wind}, m/s$	2.10	2.10		$v_{wind}, m/s$	2.45	2.45	
$ACH, 1/h$	0.34	2.64		$ACH, 1/h$	0.40	1.40	
$\eta, \%$	–	23.18		$\eta, \%$	–	25.94	
$\Psi, kg_{CO_2}/m^3/year$	–	1581.96		$\Psi, kg_{CO_2}/m^3/year$	–	846.99	

81.76 (W/m^2)/m^2. This phenomenon creates a trade-off within the TOPSIS algorithm to sacrifice the environmental emissions at better values of the number of air changes and energy efficiency.

The lowest environmental emissions are noted in the continental climatic zone because it also has the lowest geometric dimensions of the solar chimney. The highest efficiency is obtained in the tropical climatic zone, followed by the dry climatic zone due to high incident radiation.

While comparing the results with the base case conditions, it can be noted that the geometrical characteristics of the base case conditions of the solar chimney do not even meet the minimum requirements of ASHRAE standard 62. Through the optimization of the solar chimney, the number of air changes is increased by 83.4%, 81.69%, 87.12%, and 71.42% for tropical, dry, temperate, and continental climatic zone, respectively.

Another interesting point of discussion is related to the comparison between the computational time to run the multiobjective optimization using the MLP-ANN digital twin model with respect to the iterative physical model. The total computational time to run the multiobjective optimization using the original physical model for all four climatic zones is 270 min for a total of 636 iterations in the optimization results with 96,000 times of calling the function in total. On the other hand, the total computational time using the digital twin model was just 16 min for the same number of iterations and function count. The computational cost of the original physical model is too high because, for each function call (96,000) times, the physical model needs to solve the iterations on temperatures of different surfaces ($T_g^{i+1}, T_f^{i+1}, T_w^{i+1}, T_r^{i+1}$) which does not even have a benefit for the optimization results. In total, each function call consists of an average of 84 iterations, to reach the convergence criteria, making up a total of 8,064,000 times to run the code. Thus, with this, it is proved that the digital twin model is computationally efficient with a negligible loss on the accuracy of the results.

3.4. Global projection of optimized performance of the solar chimney

The idea behind the global scale projection of the performance of an energy system, i.e., solar chimney, in this case, is to understand the macro impact of energy systems. Generally, an energy system is optimized in a research procedure, and its performance is evaluated for the local dynamics. However, the final objective of any research is the implementation within the social sector of society. For this purpose, any energy system would be produced at a level of mass scale with its factories all around the world. Thus, it is crucial to test any proposed energy system on a global scale because its mass-scale production can also yield mass-scale social, environmental, economic, and political impacts. In this way, any global projection of a micro-scaled energy system can provide insights to the global organizations, policymakers, and governments to make the decisions in the international, national and local energy transition policy.

Such global projections of the performance indicators of the energy systems have gained popularity in recent years. Fasihi et al. [52] investigated the global potential of green ammonia production utilizing an optimized configuration hybrid PV-wind power plant. The study has impacts because ammonia is one of the most used feedstocks globally and it is significant to understand its global production chain to attain decarbonization in the ammonia production sector for carbon-neutral energy systems. Ascencio-Vásquez et al. [53] provided a methodology to provide worldwide maps of the performance of solar panels using Köppen-Geiger climatic classification considering the massive global productions of solar panels worldwide. Tariq et al. [54] have formulated this concept by providing an extensive methodology to understand the global water footprints of air conditioning devices on a worldwide scale. The methodology to globally project the performance of an energy system is quite simple, however, it is quite laborious. Once the corresponding simulation model of the energy system is developed that would replicate the approximate performance of the actual physical system into a computer simulation environment, then this software package is used to conduct the studies for all possible regions worldwide. This can have a certain level of resolution which could be based upon the city, region, provinces or states, countries, or also based upon a climatic classification. Each region brings its unique set of climatic characteristics which must be placed in the computer simulation code. These characteristics can also be economical like discount rate, and inflation

rate which can bring more complexities to the global projection. In case, if the required regional data for a certain patch on the global map is not available, then the contours of the performance indicators are filled there based upon the interpolation from the surrounding regions. Finally, all the data related to the performance indicators are plotted on a global map through computer graphics software.

Considering this background, the optimized performance of the solar chimney is also projected on a global scale (Fig. 6) and it is correlated with some major global problems outlined in Table 4. This analysis has quite a depth of discussion. Certain countries in the world like India, Pakistan, Bangladesh, Ethiopia, Nigeria, Kenya, etc., have some of the highest population density in the world (Table 4). Furthermore, these countries are also relatively hot on the global ambient temperature scale. However, unfortunately, the buildings of these countries are not equipped with air conditioning systems like in Europe or North America. This is a worrisome situation because their future ambient temperature will increase even more owing to global warming. In fact, some recent extreme heatwaves in Karachi, Pakistan took away more than 65 people [55]. Likewise, the heatwave in India has taken way the lives of around 36 people [56]. That is why these regions also have some of the highest growth in air conditioners. Furthermore, it is also estimated (Table 4) that their residential sector heating and cooling energy consumption in the building sector would increase by a significant percentage by the mid-century. Unfortunately, many of these countries also have dubious status on the building energy codes. This is also somewhat reflected in the concepts of energy and climate change injustice because these countries suffer the most from climate change even though their participation in climate change is lowest as compared to the European or North American countries. Even though, these countries do not have the highest current environmental impacts of the air conditioning sector but it may increase by many folds in the coming decades if their thermal management problem of the building would be left unresolved. In this case, the number of air changes per hour (Fig. 6a) through using a solar chimney in a number of these vulnerable countries complies with the ASHRAE ventilation standard 62. Likewise, the energy efficiency of the solar chimney in these countries also ranges between 29 and 32% (Fig. 6b) which is higher as compared to other regions in the continental climatic zone. Moreover, the usage of the solar chimney can also mitigate the environmental influence of conventional air conditioning by a range between 1000 and 1600 kg_{CO2}/m_3/year. In other words, it can be said that these set of likewise countries are still in the first phase of the usage of air conditioning devices where the objective is to install maximum air conditioning units. Thus, this is the best time for these countries to start including other mandatory passive components in the buildings to decrease the energy intensity of the new buildings. Thus, it is highly recommended for these and other likewise countries to include passive cooling systems i.e., solar chimneys in their national energy transition plan applied to the building energy sector.

On the other hand, several countries in Europe and North America have well-developed norms and standards on the building energy sector. The growth of air conditioners in these sectors is also medium, reflecting that these countries already have sufficient conditioned built environment to satisfy a high percentage of their population. Thus, these countries are in the second phase of using air conditioning devices where the intention is to improve the energy efficiency of existing systems. In this case, the renovation of existing buildings through the usage of solar chimneys can still improve the thermal comfort of the built environment. Noting from Fig. 6, the number of air changes and energy efficiency is also considerable for these countries. Thus, it is also recommended for these and likewise countries to include passive cooling systems i.e., solar chimneys in their national energy transition plan applied for the renovation of existing buildings or in the construction of new buildings.

There is also a somewhat interesting perspective of these recommendations which has prime importance. By the social norms and customs, it is a common practice by the constructors not to consider the significant passive systems in the buildings apart from the usage of ventilated buildings and possibly reflective materials on the roof of the residential building. Planning a futuristic standard with an obligation to include some of the passive systems in the residential buildings can cause social resistance among the society. Thus, it is necessary to provide mass education and training programs to society on the details, usage, application, maintenance, and benefits of passive systems to the common to better implement a building energy standard with obligatory passive components.

Conclusion

This research has focused on three aspects of the integration of a solar chimney with a building. The first one is to translate the physical model into an empirical, digital twin, metamodel, or surrogate model. The second is to carry out a multiobjective optimization for trade-off results between the maximized energy efficiency and a number of air changes and minimized environmental emissions. The third one is to project the optimal performance of solar chimneys on the global map and correlate it with various other global indicators. Following are the principal conclusions:

a. The influence of the parameters related to building envelope parameters and the occupants such as: $\dot{q}_{gen}, U_{t,wall,construction}, U_{t,roof,construction}, U_{t,floor,construction}, U_{door,construction}, U_{window,construction}$ is minimal in which the performance indicators change by only ~1%–~10% while changing these parameters by more than eight times.
b. The coefficient of determination R^2 of air changes per hour (ACH), energy efficiency (η), and specific environmental influence (Ψ) using multivariate regression method based on least square regression method involving the higher-order terms and interactions between the variables is 0.9881, 0.7062, and 0.9881, respectively.
c. The coefficient of determination R^2 of air changes per hour (ACH), energy efficiency (η), and specific environmental influence (Ψ) using multilayer perceptron artificial neural network is 0.9881, 0.9894, and 0.9881, respectively.
d. A comparative analysis between the multivariate regression method and multilayer perceptron artificial neural network has shown that the latter offers a better regression fit between the input parameters and the output parameters.
e. Non-dominated sorting genetic algorithm and Technique for Order of Preference by Similarity to Ideal Solution (TOPSIS) has provided the following optimal solutions:
   i. For tropical climatic zone: $L = 5m, W = 1.7m, d = 0.3m$ providing $T_a = 307.8K, I_T = 695W/m^2, v_{wind} = 3.61m/s$ which yield $ACH = 2.31/h, \eta = 31.3\%, \Psi = 1379.8kg_{CO_2}/m^3/year$.
   ii. For dry climatic zone: $L = 6m, W = 3.5m, d = 0.05m$ providing $T_a = 307.66K, I_T = 753W/m^2, v_{wind} = 2.13m/s$ which yield $ACH = 2.13/h, \eta = 28.09\%, \Psi = 1158.1kg_{CO_2}/m^3/year$.
   iii. For temperate climatic zone: $L = 5m, W = 3.3m, d = 0.14m$ providing $T_a = 300.96K, I_T = 498W/m^2, v_{wind} = 2.64m/s$ which yield $ACH = 2.64/h, \eta = 23.18\%, \Psi = 1581.96kg_{CO_2}/m^3/year$.
   iv. For continental climatic zone: $L = 3.5m, W = 2.4m, d = 0.1m$ providing $T_a = 298.26K, I_T = 799W/m^2, v_{wind} = 2.45m/s$ which yield $ACH = 1.401/h, \eta = 25.94\%, \Psi = 846.99kg_{CO_2}/m^3/year$.
f. The comparison of the base case condition with the optimized case has shown an improvement between ~71% and ~87%.
g. The optimized case condition fulfills ASHRAE standard 62 to provide an adequate ventilation rate for the building.
h. The global projection has shown that it is the need of the hour to start implementing the obligation of the usage of passive components for the new buildings and retrofit of the existing buildings to include passive components. However, education programs to the public must be offered before to avoid any social resistance.

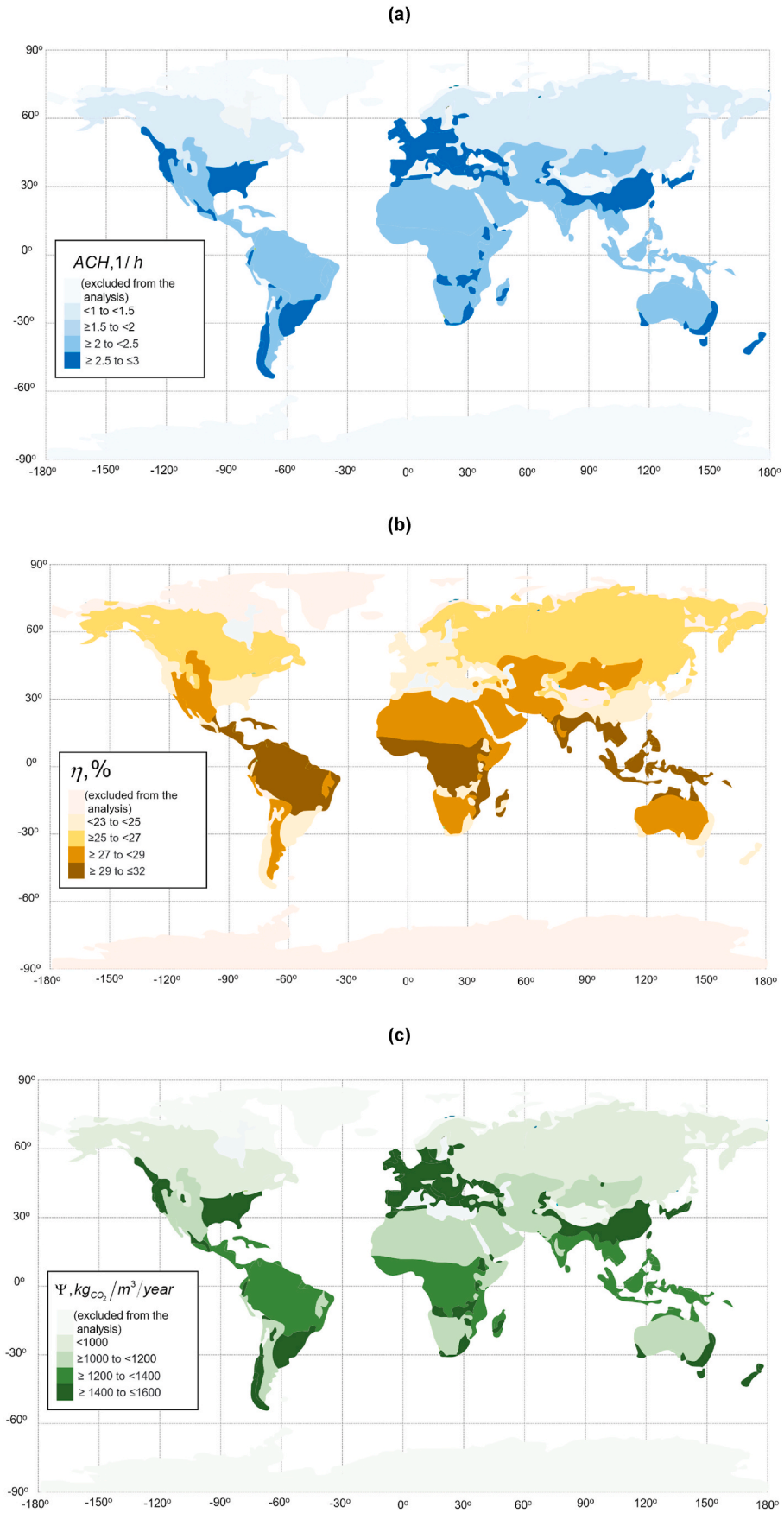

Fig. 6. Global projections of **(a)** air changes per hour (ACH), **(b)** energy efficiency (η), and **(c)** specific environmental influence (Ψ).

Table 4
Outlined global indicators of selected countries related to social, energy, economic, environmental, and political dimensions to extend the discussion related to the global projection of the performance of the solar chimney. The references used in this Table are [57–61].

Countries[1]	Population density (people/km^2) [57]	Growth of air conditioners [58]	Climate impact of the cooling sector (Megatons$_{CO2-e}$) [59]	Residential sector heating and cooling energy consumption in building sector in the year 2020 (kW/m^2) [60]	Residential sector heating and cooling energy consumption in building sector in the year 2050 (kW/m^2) [60]	Building energy codes by jurisdiction, 2017-18 [61]
India	464	High	60-1000	77.1	89.2	Mandatory for a part of sector
Pakistan	287	High	60-1000	77.1	89.2	Voluntary for part of sector
Nepal	203	High	0.07-2	77.1	89.2	No known code
China	153	High	>1000	41.2	47.5	Mandatory for entire sector
France	119	Medium	60-1000	123.1	110.4	Mandatory for entire sector
Ethiopia	115	Medium	60-1000	53.4	52.9	No known code
Turkey	110	Medium	60-1000	123.1	110.4	Mandatory for entire sector
Egypt	103	Medium	60-1000	55.1	58.0	Voluntary for part of sector
Spain	94	Medium	60-1000	123.1	110.4	Mandatory for entire sector
Kenya	94	Medium	60-1000	53.4	52.9	No known code
Iraq	93	Medium	60-1000	55.1	58.0	No known code
Morocco	83	Medium	60-1000	55.1	58.0	Mandatory for entire sector
Tunisia	76	Medium	60-1000	55.1	58.0	Mandatory for entire sector
Tanzania	67	Medium	60-1000	53.4	52.9	Code in development
Mexico	66	High	60-1000	60.2	59.6	Mandatory for a part of sector
Yemen	56	Medium	60-1000	55.1	58.0	No known code
Iran	52	Medium	60-1000	55.1	58.0	Mandatory for part of sector
South Africa	49	Medium	60-1000	53.4	52.9	Voluntary for part of sector
Mozambique	40	Medium	60-1000	53.4	52.9	No known code
Zimbabwe	38	Medium	60-1000	53.4	52.9	No known code
U.S.	36	High	60-1000	138.4	119.7	Mandatory and voluntary
Chile	26	Medium	60-1000	60.2	59.6	Mandatory for a part of sector
Peru	26	Medium	60-1000	60.2	59.6	No known code
Sudan	25	Medium	60-1000	53.4	52.9	No known code
Somalia	25	Medium	2-60	53.4	52.9	No known code
Niger	19	Medium	60-1000	53.4	52.9	No known code
Algeria	18	Medium	60-1000	55.1	58.0	No known code
Mali	17	Medium	60-1000	53.4	52.9	No known code
Argentina	17	Medium	60-1000	60.2	59.6	Mandatory for a part of sector
Saudi Arabia	16	Medium	60-1000	55.1	58.0	Voluntary for part of sector
Oman	16	Medium	60-1000	55.1	58.0	No known code
Chad	13	Medium	60-1000	53.4	52.9	No known code
Russia	9	Medium	60-1000	198.4	191.6	Mandatory for entire sector
Kazakhstan	7	Medium	60-1000	198.4	191.6	Mandatory for entire sector
Libya	4	Medium	60-1000	55.1	58.0	No known code
Botswana	4	Medium	2-60	53.4	52.9	No known code
Australia	3	High	60-1000	122.4	113.4	Mandatory for entire sector
Namibia	3	Medium	2-60	53.4	52.9	No known code

CRediT authorship contribution statement

Rasikh Tariq: Conceptualization, Data curation, Formal analysis, Funding acquisition, Investigation, Methodology, Project administration, Resources, Software, Supervision, Validation, Visualization, Writing – original draft, Writing – review & editing. **C.E. Torres-Aguilar:** Writing – review & editing, Validation, Supervision, Software, Formal analysis. **J. Xamán:** Funding acquisition, Resources, Supervision, Writing – review & editing. **I. Zavala-Guillén:** Writing – review & editing, Supervision, Resources, Funding acquisition. **A. Bassam:** Conceptualization, Funding acquisition, Resources, Supervision, Writing – review & editing. **Luis J. Ricalde:** Writing – review & editing, Supervision, Resources, Project administration, Writing – review & editing, Funding acquisition. **O. Carvente:** Conceptualization, Funding acquisition, Project administration, Supervision, Writing – review & editing.

Declaration of competing interest

The authors declare that they have no known competing financial interests or personal relationships that could have appeared to influence the work reported in this paper.

Acknowledgment

The author, Rasikh Tariq, is grateful to the financial support of CONACYT (*Consejo Nacional de Ciencia y Tecnología*) to pursue a *Doctorado en Ingeniería opción Energías Renovables* in *Facultad de Ingeniería, Universidad Autónoma de Yucatán* with the CVU: 949314, scholarship no: 784785, and program: *becas nacionales*.

Appendix A. Missing sections of research method

A.1. Description of terms involved in the physical model of building-integrated solar chimney

See Table A.I.

Table A.I
Description of terms involved in the physical model of building-integrated solar chimney.

Source of equation:	Description of terms:
Eq. (1)	a. $S_1 = \alpha_1 I_T$. I_T is the total solar radiation on the vertical surface of the solar chimney subject to the day of the year, the hour of the day, latitude, and longitude, given by: $I_T = I_b R_b + I_d\left(\frac{1+\cos\beta}{2}\right) + (I_b + I_d)\rho_g\left(\frac{1-\cos\beta}{2}\right)$. Here, β is the tilt angle which is 90° for the vertically oriented glass of the solar chimney. R_b is the title factor, for the northern hemisphere for a south-facing solar chimney, the tilt factor is given by: $R_b = \frac{\cos(\phi-\beta)\cos\delta\cos\omega + \sin(\phi-\beta)\sin\delta}{\cos\phi\cos\delta\cos\omega + \sin\phi\sin\delta}$. ϕ is the latitude of the subject location. δ is the declination angle of Earth which is given by: $\delta = 23.45\sin\left(360\frac{284+\text{Day of the year}}{365}\right)$. ω is the hour angle which is zero degrees at solar noon. It changes in negative and positive before and after the solar noon, respectively, by 15° representing each hour of the day. I_b and I_d are direct and diffused part of the solar radiation. ρ_g is the ground reflectance which is taken as 0.6 [62].
	b. $h_{r,w-g}$ is the radiative heat transfer coefficient between the wall and glass: $h_{r,w-g} = \frac{\sigma(T_g^2+T_w^2)(T_g+T_w)}{\frac{1}{\varepsilon_g}+\frac{1}{\varepsilon_w}-1}$.
	c. $h_{c,f-g}$ is the convective heat transfer coefficient between the fluid (air) and the glass. It is obtained through the Nusselt number using $h_{c,f-g} = \frac{Nu_{f-g}k_f}{L}$. The airflow is natural convection driven by the buoyancy force. The ratio of the buoyancy to the viscous force i.e., Grashof number, would determine the flow regime (laminar or turbulent). It is given by: $Gr = g\beta_f(T-T_f)L^3/\nu^2$. The variable T in the Grashof number can refer to T_g for $h_{c,f-g}$. It is converted into the ratio of buoyancy and viscosity forces multiplied by the ratio of momentum and thermal diffusivities, i.e., Rayleigh number using $\text{Re} = Gr\,\text{Pr}$. The following correlation is applicable in the laminar region with a Rayleigh number less than 10^9: $Nu = 0.68 + 0.670Ra^{\frac{1}{4}}/\left(1+(0.492/\text{Pr})^{\frac{9}{16}}\right)^{\frac{4}{9}}$ [63]. For Rayleigh's number greater than 10^9, the following correlation is valid: $Nu = \left[0.825 + 0.387Ra^{\frac{1}{6}}/\left(1+(0.492/\text{Pr})^{\frac{9}{16}}\right)^{\frac{8}{27}}\right]^2$ [63].
	d. The total heat loss coefficient $(U_t)$from the solar chimney is given by: $U_t = h_{wind} + h_{r,g-s}$. Here, convective heat transfer due to wind is given by: $h_{wind} = 5.7 + 3.8v_{wind}$ [64]. $h_{r,g-s}$ is the radiation heat transfer coefficient from the top glass surface to the sky and is expressed in the form: $h_{r,g-s} = \sigma\varepsilon_g(T_g+T_s)(T_g^2+T_s^2)(T_g-T_s) \div (T_g-T_a)$ where T_s is the sky temperature and can be written in the form of ambient temperature using: $T_s = 0.0552T_a^{1.5}$ [65].
Eq. (2),	a. $h_{c,w-f}$ is the convective heat transfer coefficient from the wall to the fluid (air). It has the same calculation procedure as $h_{c,f-g}$. However, $h_{c,w-f}$ is different from $h_{c,f-g}$ because the variable T in the Grashof number can refer to T_w for $h_{c,w-f}$.
	b. The term $\dot{q}''$ in eq. (2) is the rate of heat transfer entering the fluid. It can be determined through an energy balance at an inlet and outlet of the air channel, given by the equation: $\dot{q}''WL = \dot{m}c_f(T_{f,o} - T_{f,i})$. It is desired to eliminate the outlet fluid air temperature because it is an unknown quantity, and it can be replaced with a thermal shape factor (γ). Thus, it is given by: $T_f = \gamma T_{f,o} + (1-\gamma)T_{f,i}$. The physical significance of the thermal shape factor is that it gives the relationship between the inlet fluid temperature and the outlet fluid temperature. It can be re-arranged to give the outlet fluid temperature as: $T_{f,o} = \frac{T_f - (1-\gamma)T_{f,i}}{\gamma}$. Plugging it into the equation of $\dot{q}''$, we get: $\dot{q}'' = \frac{\dot{m}c_f}{\gamma WL}(T_f - T_{f,i}) = M(T_f - T_{f,i})$ with $M = \frac{\dot{m}c_f}{\gamma WL}$. In this case, correlation to find the mass flow rate is used which is: $\dot{m} = C_d\frac{\rho_{f,o}A_o}{\sqrt{1+A_r}}\sqrt{\frac{2gL(T_f-T_r)}{T_r}}$ in which $C_d = 0.6$ [66]. The inlet (A_i) and the outlet area (A_o) are the same i.e., rectangular channels calculated using: $A_o = A_i = dW$. The area ratio (A_r) is $A_r = A_o/A_i$.
Eq. (3)	a. S_2 is the solar radiation heat flux absorbed by the black absorber plate. It is given by: $S_2 = \tau\alpha_2 I_T$.
	b. $U_{t,w-r}$ is the overall heat transfer coefficient from the rate of the vertical wall to the room. It is given by: $U_{t,w-r} = \left[\frac{1}{h_r} + \frac{\Delta w_{ins}}{k_{ins}}\right]^{-1}$. Here, h_r is the convective heat transfer coefficient between the vertical wall and the interior of the room. It can be considered equal to 10 W/(m^2.K) [67].
Eq. (4)	a. $U_{t,leftwindow} = U_{t,frontwindow} = U_{t,rightwindow} = U_{t,backwindow} = U_{t,backventilation,window} = \left[\frac{1}{h_{wind}} + \frac{1}{U_{window,construction}} + \frac{1}{h_r}\right]^{-1}$
	b. $U_{t,leftwall}^{withoutsolarchimney}$ is the total heat transfer coefficient from the interior of the room to the ambient condition from the left wall area where the solar chimney is not connected, given by: $U_{t,leftwall}^{withoutsolarchimney} = \left[\frac{1}{h_{wind}} + \frac{1}{U_{t,wall,construction}} + \frac{1}{h_r}\right]^{-1}$.
	c. $U_{t,leftwall}^{withoutsolarchimney} = U_{t,frontwall} = U_{t,rightwall} = U_{t,backwall}$
	d. $U_{t,door} = \left[\frac{1}{h_{wind}} + \frac{1}{U_{door,construction}} + \frac{1}{h_r}\right]^{-1}$
	e. $U_{t,roof} = \left[\frac{1}{h_{wind}} + \frac{1}{U_{t,roof,construction}} + \frac{1}{h_r}\right]^{-1}$, $U_{t,floor} = \left[\frac{1}{h_r} + \frac{1}{U_{t,floor,construction}}\right]^{-1}$

A.2. Solution methodology

The objective to solve the energy balance equations is to calculate the values of T_g, T_f, T_w, and T_r, and the values of the heat transfer coefficients are also based upon the values of T_g, T_f, T_w, and T_r. The mathematical model is written in terms of the temperature of each system by using a first-order accurate finite difference formulation scheme. The current problem exposes as a coupled problem where an iterative solution must be adapted. For this purpose, initial values of these temperatures are assumed $(T_g^i, T_f^i, T_w^i, T_r^i)$. The transport properties are calculated using the assumed temperatures $(T_g^i, T_f^i, T_w^i, T_r^i)$. Afterward, the new values of the temperatures $(T_g^{i+1}, T_f^{i+1}, T_w^{i+1}, T_r^{i+1})$ are calculated using the energy balance equations through their solution using the Gauss-Seidel method. This iteration loop is repeated until a convergence criterion is attained. The convergence is monitored by calculating the error in each successive iteration of each temperature $(T_g^{i+1}, T_f^{i+1}, T_w^{i+1}, T_r^{i+1})$. The error of the successive iteration on the glass cover temperature is calculated using: $error_{T_g} = \left|T_g^{i+1} - T_g^i\right| / T_g^i$. The total iterative error is the sum of each error given by: $error_{total} = error_{T_g} + error_{T_f} + error_{T_w} + error_{T_r}$. The iterations are stopped when the following convergence criteria are attained: $error_{total} < 1.0e-12$.

A.3. Validation of the physical model

The validation of the physical model is conducted by comparison with the results of a highly-cited and one of the pioneer mathematical models of solar chimney published by Ong [66]. One of the benefits of validating with the physical model of Ong [66] is that such validation would bring the current work to the existing pool of published research articles. For example, Arce et al. [67] validated the thermal performance of a small solar chimney installed in a building with the model of Ong [66]. Belfegas et al. [68] carried out an experimental and theoretical investigation of a solar chimney for the ventilation purposes of a living room and the authors also validated their model with Ong [66].

The author used a physical model of a solar chimney like a Trombe wall. The chimney consisted of a glass cover which with the other three solid walls of the chimney form a channel through which the heated air could rise and flow by natural convection. The opening was provided at the bottom and the top of the chimney to allow the room air to enter and leave the channel. The author developed steady-state heat transfer equations using a thermal resistance network along with appropriate boundary conditions on the surface of the glass cover, heat-absorbing wall, and airflow. A matrix-inversion solution procedure was adapted, and the performance was reported using the temperatures of different surfaces and fluids, air mass flow rate, and instantaneous heat collection efficiency. Marti-Herrero et al. [69] also studied the dynamic physical model for a solar chimney and compared their findings with the results of Ong [66]. In fact, the model of Ong [66] also supports other pioneer articles in this area, like the one published by Hirunlabh et al. [70].

However, one of the differences between the research design of Ong [66] and the current work is that Ong [66] did not consider the integrated model of the building with the solar chimney. In fact, Ong [66] only solved the physical model of the solar chimney in which the ambient air conditions were considered the same as the inlet of the solar chimney. However, in reality, it would not be true because the inlet of the solar chimney is actually room temperature. Thus, in this case, the boundary conditions of the physical model of Ong [66] are different from the current work. Consequently, for validation purposes, the current model is bought in the same boundary conditions as the one solved by Ong [66]. Apart from this, all the variables used by Ong [66] are used for the solution of the physical model. It involved the transmittance, emittance, absorptance, thickness of the glass, distance from the glazing to the wall, width of the solar chimney, thermal heat resistance of the back wall, emittance of the back wall, ambient temperature, and wind velocity. The variables in this validation study are the length of the solar chimney (or wall length), and the incoming solar radiation.

Fig. A1 (a and b) shows the influence of changing wall length on the temperatures, efficiency, and mass flow rate. It can be noted that apart from the efficiency, all other indicators including the glass temperature, wall temperature, fluid temperature, fluid outlet temperature, change in the fluid temperature, and mass flow rate, increase with the increase in the wall length. It is because the increase in the wall-length also increases the exposed solar radiation capturing area which increases the glass temperature, wall temperature, fluid temperature, and fluid outlet temperature. Consequently, it enhances the upward pressure suction in the solar chimney resulting in a high mass flux. Eventually, it decreases the efficiency because the length is in the denominator of the formula of efficiency. Physically, it signifies that the increase in the wall-length increases the incoming useful heat input (WLI_T) which does not meet the increase in the required output $(\dot{m}c_f(T_{f,o} - T_{f,i}))$. A fluctuation is also noted in the variables when the wall length is changed from 0.8 m to 1 m, representing the transition region when the equations of the Rayleigh number are shifted from the laminar to turbulent natural convection.

Fig. A1 (c and d) shows the influence of the increasing solar radiation on the temperatures, efficiency, and mass flow rate, and their increase also increases in all the performance indicators. At low incident solar radiation levels, the temperature of the front glass is lower than the mean fluid temperature and the outlet air temperature. At higher solar radiation, it is higher than the mean fluid temperature and the outlet air temperature. The parameters including glass temperature, wall temperature, fluid temperature, fluid outlet temperature, change in the fluid temperature, mass flow rate, and efficiency are increasing with the increase in solar radiation because a higher solar radiation impulses the overall system with its heat.

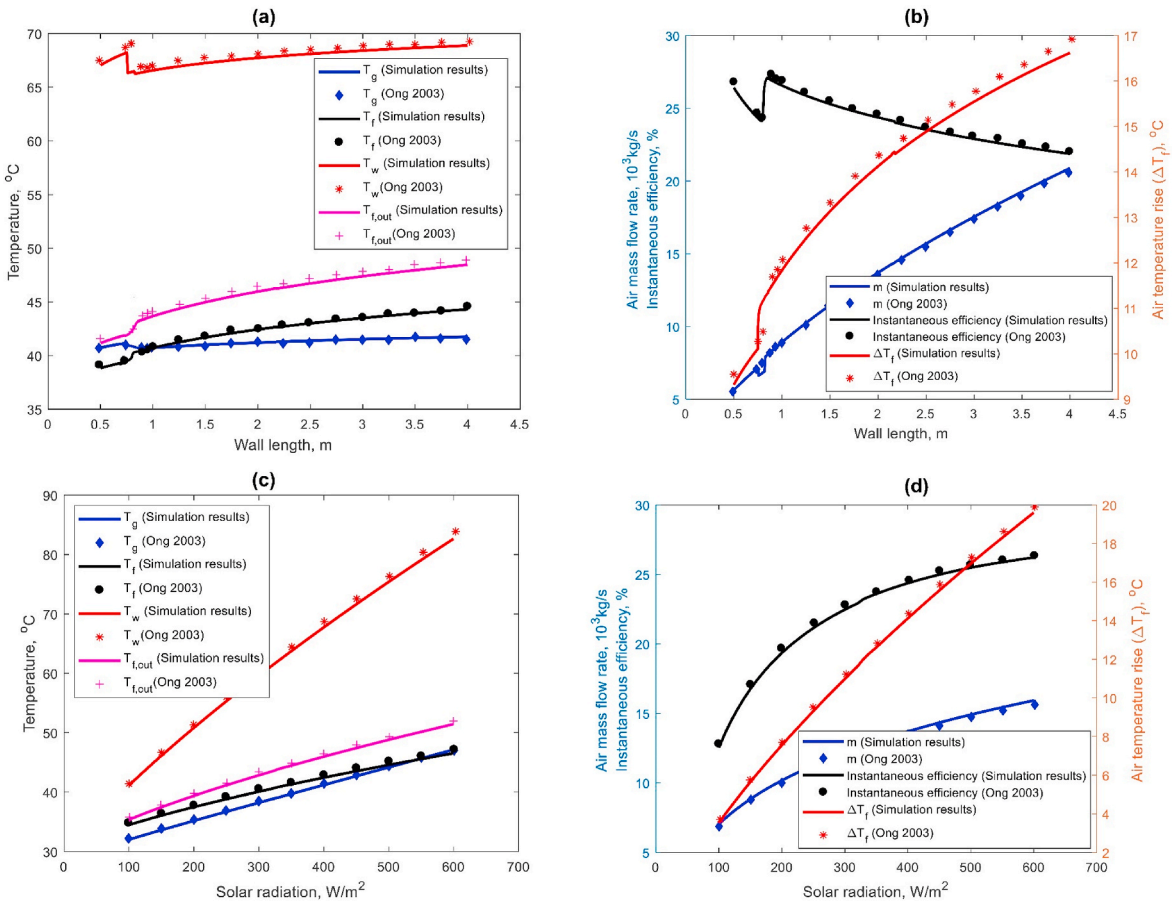

Fig. A.1. Validation of the results by comparison with the findings of Ong [66]. Influence of changing the wall length on (a) temperatures of different fluids and surfaces, and (b) some basic performance indicators. Influence of changing solar radiation on (c) temperatures of different fluids and surfaces, and (d) some basic performance indicators.

A.4. Description of case study

The construction of the built environment consists of a 12x12 × 3.0 m single-story residential house (see Fig. 1a). It consists of a living room, three bedrooms, a kitchen, and a bathroom. Such a small-scale construction is also known as alternatively "social house (or low-income housing)" [71–76]. The front wall consists of a door with dimensions 0.90 × 2.10 m, and two main windows each have 1.20 × 1.50 m dimensions. The windows on the front wall refer to the kitchen and the living room. The right-side wall consists of three windows of the same dimensions opening to the kitchen, and the two bedrooms. The backside consists of two standard windows for the two bedrooms, and two small ventilation windows for the bathroom having dimensions 1.0 × 0.3 m. The left side wall consists of a single standard window for the third living room, and a solar chimney. The building is attached to the solar chimney through an opening from the house. The left side wall is assumed to be south-facing for the northern hemisphere and north-facing for the southern hemisphere. It is also assumed that there is no effect of surrounding shadow on the building to simplify the problem.

Table lists down the details and characteristics of the selected cities within each classification of the climatic zone (under Köppen-Geiger climatic classification) along with the architectural and air conditioning load conditions. The design dry-bulb temperature is taken from ASHRAE [77] at 0.4% design conditions which signifies that the temperature in a typical year for that location will exceed this design value for about 0.4% of the time. The radiation data is also taken from the ASHRAE database by taking a monthly average of all the months of clear sky solar irradiance. The wind velocity is taken from the Global Wind Atlas which is a platform developed in collaboration with the World Bank Group, Energy Sector Management Assistance Program, Vortex group, and Technical University of Denmark [78]. The minimum height for the data of average wind velocity on this platform is 10 m which is accepted. Other details are displayed in Table A.II.

Table A.II
Simulation data and additional formulas related to the geometry, heat transmission, and the internal load of the building, solar chimney, and thermophysical properties. The table also specifies the outdoor weather conditions of selected cities under the Köppen-Geiger classification.

(a) Architectural details, air-conditioning load conditions of the building, along with other parameters.

No.	Variable	Details
	The geometry of the building	
1	Length of the building	12 m
2	Width of the building	12 m
3	Height of the building	3 m
4	Area of the floor and roof	

(*continued on next page*)

Table A.II (*continued*)

(a) Architectural details, air-conditioning load conditions of the building, along with other parameters.

No.	Variable	Details
		$A_{t,roof} = A_{t,floor} = 12 \times 12 = 144m^2$
5	Area of the wall	$A_{t,leftwall} = A_{t,frontwall} = A_{t,backwall} = A_{t,rightwall} = 12 \times 3 = 36m^2$
6	Dimensions of the normal window	$A_{window} = 1.5 \times 1.5 = 2.25m^2$
7	Area of the ventilation windows	$A_{ventilation,window} = 1 \times 0.3 = 0.3m^2$
8	Dimensions of the door	$A_{door} = 2.1 \times 0.90 = 1.89m^2$
9	Area of the solar chimney (variable)	$A_{solarchimney} = WL$
	Heat transmission	
10	Heat transfer coefficient of the floor construction	$U_{t,floor} = 0.13W/m^2.K$ [79]
11	Heat transfer coefficient of the roof construction	$U_{t,roof} = 0.13W/m^2.K$ [79]
12	Heat transfer coefficient of the construction of the external wall	$U_{t,wall,construction} = 0.18W/m^2.K$ [79]
13	Heat transfer coefficient of the door construction	$U_{door,construction} = 1.2W/m^2.K$ [79]
14	Heat transfer coefficient of the window construction	$U_{window,construction} = 1.4W/m^2.K$ [79]
	Internal load	
15	Internal load generation[1]	$\dot{q}_{gen} = 1089W$
	Thermophysical and constant parameters and formulas	
16	Convective heat transfer coefficient of the room	$h_r = 10W/m^2.K$
17	Thermal conductivity of the insulation	$k_{ins} = 0.0275W/m.K$
18	Absorptivity of glass	$\alpha_1 = 0.06$
19	Absorptivity of wall	$\alpha_2 = 0.95$
20	Emissivity of the outer surface of the glass	$\varepsilon_g = 0.90$
21	Emissivity of the black wall surface	$\varepsilon_w = 0.94$
22	Thickness of the insulation	$\Delta w_{ins} = 0.022m$
23	Stefan-Boltzmann constant	$\sigma = 5.67 \times 10^{-8} W/m^2 \cdot K$
24	Transmittivity of glass	$\tau = 0.84$
25	Temperature dependent dynamic viscosity of air[2]	$\mu_f = [1.846 + 0.00472(T_f - 300)] \times 10^{-5}$(Valid for $300 - 350K$)
26	Temperature dependent density of air[2]	$\rho_f = 1.1614 - 0.00353(T_f - 300)$(Valid for $300 - 350K$)
27	Temperature dependent specific heat of air[2]	$c_{p,f} = [1.007 + 0.00004(T_f - 300)] \times 10^3$(Valid for $300 - 350K$)
28	Temperature dependent thermal conductivity of air[2]	$k_f = 0.0263 + 0.000074(T_f - 300)$(Valid for $300 - 350K$)
29	Volumetric coefficient of expansion	$\beta = {}^{1}/_{T_f}$
30	Prandtl number	$\mathrm{Pr} = c_{p,f}\mu_f / k_f$
31	Kinematic viscosity	$\nu_f = \mu_f / \rho_f$

(b) Specifications of outdoor weather conditions

No.	Specification	Details	Reference
	Mumbai, India		
1	Köppen-Geiger classification	Tropical	[80]
2	Coordinates	(19.12 N, 72.85E)	[77]
3	Monthly-averaged annual design dry-bulb temperature (0.4%)	34.7 °C (307.8 K)	[77]
4	Monthly-averaged annual design wet-bulb temperature (0.4%)	26.7 °C	[77]
5	Monthly-average annual clear sky solar irradiance	695.0 W/m^2	[77]
6	Wind velocity[3]	3.61 m/s	[78]
	Cairo, Egypt		
1	Köppen-Geiger classification	Dry	[80]
2	Coordinates	(30.13 N, 31.40E)	[77]
3	Monthly-averaged annual design dry-bulb temperature (0.4%)	34.5 °C (307.66 K)	[77]
4	Monthly-averaged annual design wet-bulb temperature (0.4%)	18.8 °C	[77]
5	Monthly-average annual clear sky solar irradiance	753.0 W/m^2	[77]
6	Wind velocity	1.94 m/s	[78]
	Shanghai, China		
1	Köppen-Geiger classification	Temperate	[80]
2	Coordinates	(31.40 N, 121.47E)	[77]
3	Monthly-averaged annual design dry-bulb temperature (0.4%)	27.8 °C (300.96K)	[77]
4	Monthly-averaged annual design wet-bulb temperature (0.4%)	20.53 °C	[77]
5	Monthly-average annual clear sky solar irradiance	498.0 W/m^2	[77]
6	Wind velocity	2.1 m/s	[78]
	New York, United States		
1	Köppen-Geiger classification	Continental	[80]
2	Coordinates	(40.66 N, 73.8W)	[77]
3	Monthly-averaged annual design dry-bulb temperature (0.4%)	25.1 °C (298.26 K)	[77]
4	Monthly-averaged annual design wet-bulb temperature (0.4%)	17.7 °C	[77]
5	Monthly-average annual clear sky solar irradiance	799 W/m^2	[77]
6	Wind velocity	2.45 m/s	[78]

[1] The internal load generation is estimated based upon the heat gain from the four adult occupants in seated, very light work conditions along with an approximated load from the electrical appliances.

[2] Reference from Refs. [81–83].
[3] Mean wind speed at a height of 10 m.

A.5. Digital twin model using least-square method based multivariate regression

The regression method is the usage of statistical tools to estimate the relationship between the set of the dependent variables with a set of the independent variables. There is a family of regression methods varying from linear, polynomial, stepwise, and logistic regression. In this work, a polynomial variation of the multivariate regression method with the interaction between the input variables is used. It can be mathematically written as: $Y_i = C^o + \sum_{i=1}^{n} C_i^1 X_i + \sum_{i=1}^{n}\sum_{j=1}^{n} C_{ij} X_i X_j + \ldots + \sum_{i=1}^{n}\sum_{j=1}^{n}\ldots\sum_{q=1}^{n} C_{ij}\ldots \underbrace{[X_i X_j \ldots X_n]}_{\text{higher order terms}} + e_i$. In this equation, Y_i is one of the three performance indicators. The term C^o is the constant in the model which is taken as zero because of a lack of interpretation in the case of the multivariate regression method. The term $\sum_{i=1}^{n} C_i^1 X_i$ represents the linear relationship between the variable X_i and Y through its weight C_i^1. The term $\sum_{i=1}^{n}\sum_{j=1}^{n} C_{ij} X_i X_j$ shows the relationship between two different input variables X_i and X_j with Y_i through its weight C_{ij}. The term $\sum_{q=1}^{n} C_{ij}\ldots \underbrace{[X_i X_j \ldots X_n]}_{\text{higher order terms}}$ represents the higher-order terms of the input variables. The term e_i represents the lack of fit between the actual performance indicator and the predicted performance indicator. The weights in the multivariate regression equations are calculated using the least square method.

A.6. Digital twin model using multilayer perceptron artificial neural network (MLP-ANN)

Artificial neural network (ANN) is an alternative to developing the digital twin of the validated physical model [84]. ANN also consists of inputs i.e., synapses (x_j), which is multiplied by the weights i.e., the strength of the respective signals (w_{kj}), as well as an external bias (b_k) which is responsible for lowering or increasing the summation's output $(y_k)$and computes a mathematical function i.e., activation of the neuron $(\varphi_{ANN}(.))$ which is applied to that output to decrease the amplitude range of the output signal (y_k). The activation function determines the threshold of a particular input neuron. This yields a particular response of the simulated neural system i.e., output (y_k). A higher weight of an artificial neuron corresponds to a strongness of the input signal. Mathematically, it can be written as: $y_k = \varphi_{ANN}(\sum_{j=1}^{m}(w_{kj}x_j) + b_k)$. Here, y_k is the output, φ_{ANN} is the activation function, w_{kj} is the weight, b_k is the bias, k represents the neuron, and j represents the synapse number. Haykin et al. [85] have mentioned four different types of activation function which are (a) linear, (b) sigmoid, (c) Gaussian, and (d) Gaussian complement.

There are different ANN models, including multilayer perceptron (MLP), Elman neural network (NN), wavelet NN, and radial basis function. Elsheikh et al. [86] have reviewed a number of articles and have concluded that MLP based NN has been widely used in solar energy applications because of its simplicity in design. MLP consists of one input layer, several hidden layers, and one or more output layers. The input layer receives the data of all the design variables and transfers this information to the next layer. The neural architecture is designed in such a way that the neurons of each layer are connected with the neurons of the next layer, for example, the input layer is connected with the first hidden layer, and the last hidden layer is connected with the output layer, however, the neurons within the same layer are not connected with each other.

In summary, a linear summation of the product of the input variable and the weight with the bias is passed on to the next layer. An activation function is applied which determines the threshold i.e., importance or significance, of the input and decides to pass on to the next hidden layer or not. All of this process occurs in a unit perceptron. It is also known that a single unit perceptron can only handle linearly separable problems, thus, a set of this unit perceptron is required in the architecture to model the actual non-linear behavior of the performance indicators. This process remains in a continuous operation until reaching the predicted output. In the first run, the values of the bias and the weights are chosen randomly and as a result, there can be a huge difference between the predicted output and the actual output. This difference is gauged by the indicator mean square error. At this step, the training process of the architecture happens because of the usage of a backpropagation algorithm which eventually estimates better values of the weight and the bias function. The iteration is stopped until convergence is attained in the subsequent iterative values of the predicted performance indicator and the actual performance indicator. The stepwise description of this process is depicted in Fig. A. 2.

The mathematical formulation has explicitly proven that the values of the weights particularly influence the final results. Thus, it goes through a set of back-propagation learning algorithms (BPLA). For this purpose, the total database requires a division into three main parts (a) training, (b) validation, and (c) testing. The training database, normally 70%, is used to fit the parameters especially the weights of the architecture. There are three main algorithms for this purpose which are Levenberg–Marquardt, Bayesian Regularization, and Scaled Conjugate Gradient. The validation database, normally 15%, is used to tune the parameters of the architecture to avoid any overfit in the training process. The testing database, normally 15%, is used to ass the performance of the predictive power of the architecture.

Levenberg–Marquardt (LM) algorithm was originally developed to solve the nonlinear least-square problems and it combines the characteristics of two other numerical algorithms: the gradient descent method and the Gauss-Newton method. The gradient descent method updates the value of the parameters in the steepest descent direction when the sum of square error is reduced. The Gauss-Newton method reduces the sum of squared errors by assuming the least-squares function is locally quadratic in the parameters, and findings the minimum of this quadratic. LM algorithm uses a damping parameter. In this way, the LM algorithm acts like a Gauss-Newton method when smaller values of damping parameters are used and acts as a gradient descent method when the value of the damping parameter is high. The Gauss-Newton method presumes that the objective function is approximately quadratic in the parameters near to the optimal solution, and thus, it is more efficient when the candidate solution is in the vicinity of the optimal solution. The gradient descent method offers a fast option during the initial iteration because it takes a downhill direction and a step size. Thus, the LM method uses higher values of lambda at the beginning of the search to minimize the search space, and then, it is shifted into a Gauss-Newton method i.e., low values of lambda, in the vicinity of the optimal solution.

Before the application of the MLP-ANN for the development of digital twin, normalization can be necessary because the design variables $(L, W, d, T_a, I_T, v_{wind})$ have different scales. One option is to divide each design variable with its maximum value to normalize the variables between the value of 0–1. However, it may generate edges in the usage of the activation function of MLP-ANN [84,87–90]. Thus, generally, it is a common practice to normalize all the variables between 0.1 and 0.9, which can be done using the following equation: $X_{i,N} = 0.9 \times \frac{x_i - x_{\min}}{x_{\max} - x_{\min}} + 0.1$. Here, $X_{i,N}$ is the normalized variable between the range 0.1–0.9. x_i is the value of the variable before normalization. $x_{\min}$ and $x_{\max}$ are the minimum and the maximum

values of the input variable vector$x$. Normalization also helps to adjust the weights in the architecture of the neural network because a variable with an inherently wide range would also have a higher value of the weight. It should also be noted that the normalization process does not change the statistical distribution of the input parameters which is acceptable.

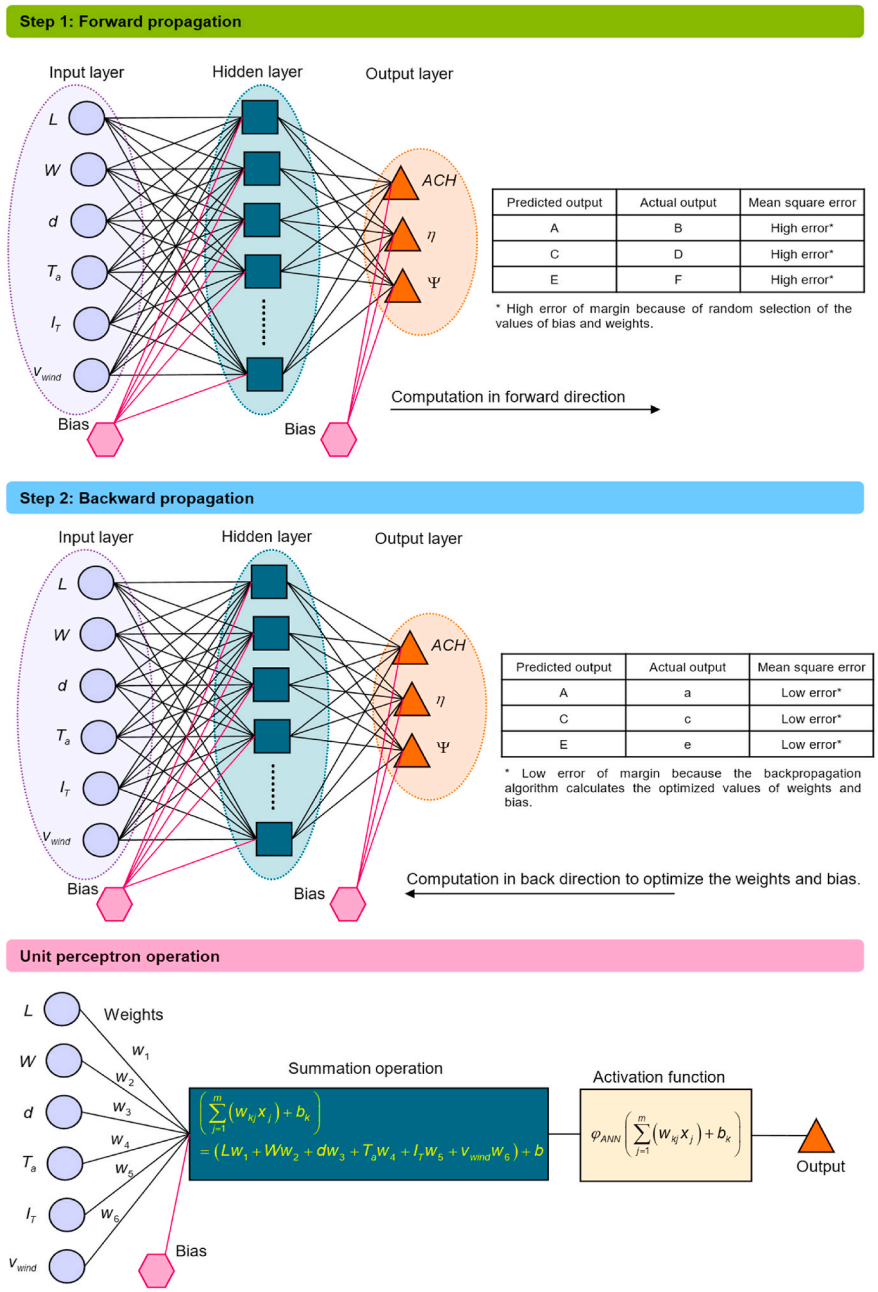

Fig. A. 2. Stepwise description of the architecture and functioning of multilayer perceptron artificial neural network for the estimation of air changes per hour (ACH), energy efficiency (η), and specific environmental influence (Ψ).

A.7. Limitations of the study

Various building-related characteristics especially the type of construction of the building envelope and the internal heat generation load can be quite sensitive before the design of the optimization problem formulation. Thus, it is deemed necessary to report that how changing these variables would influence the performance indicators. For this purpose, a sensitivity analysis of these variables ($\dot{q}_{gen}$, $U_{t,wall,construction}$, $U_{t,roof,construction}$, $U_{t,floor,construction}$, $U_{door,construction}$, $U_{window,construction}$,) on the three performance indicators is carried out in a form of parametric analysis.

The value of internal heat generation ($\dot{q}_{gen}$) is changed from 0 W to 3000 W. Here, 3000 W can show an extreme activity level of the occupants and

the heat generation from the electrical appliances for the architecture of the subject building. The results are reported in Fig. A. 3. (a), (b), and (c). It can be noted that the increase in internal heat generation decreases the number of air changes per hour. It is because the total ventilation rate ($\dot{V}_o$) (the numerator of the *ACH*) keeps on decreasing with the increased internal heat generation. The total ventilation rate depends on the difference between the fluid temperature, and the room temperature ($T_f - T_r$). Thus, in this case, the fluid temperature and the room temperature keep on increasing because of the increase in the internal heat generation. As a result, the difference between the fluid temperature and the room temperature decreases ($T_f - T_r$) with the increase in the internal heat generation. This causes a diminution in the value of the total ventilation rate ($\dot{V}_o$) with increasing internal heat generation. Consequently, the number of air changes decreases with the increase in internal heat generation. In other words, the increase in the internal heat generation decreases the ventilation potential because the natural ventilation can take less heat content from the residential building. However, increasing the $\dot{q}_{gen}$ from 0 W to 3000 W (3000 times increase) only decreases the *ACH* from ~1.24 1/h to ~1.20 1/h (~3.22% change), which indicates that the variable $\dot{q}_{gen}$ is not a highly sensitive variable for the *ACH*.

Fig. A. 3. (b) shows the influence of internal heat generation ($\dot{q}_{gen}$) on energy efficiency (η). It can be seen that the increase in internal heat generation increases energy efficiency. The energy efficiency depends on the collected heat from the solar chimney i.e., the difference of outlet and inlet fluid temperature. However, in this case, the outlet fluid temperature keeps on increasing because of the increase in the internal heat generation, consequently, the energy efficiency increases with the increase in the internal heat generation. The sensitivity of internal heat generation on the energy efficiency is minimal because changing the $\dot{q}_{gen}$ by 3000 times only changes the energy efficiency by only ~7.74% (from ~29.70% to ~32.00%). The specific environmental influence (Ψ) decreases with the increase in the internal heat generation because it also decreases the ventilation potential which is directly related to the theoretical shaft fan power. The specific environmental influence decreases from ~747.53 kg_{CO2e}/m^3/year to ~727.16 kg_{CO2e}/m^3/year (a change of ~2.72%) with a 3000 times increase in $\dot{q}_{gen}$.

Fig. A. 3. (d, g, m, and p) shows the same trend in which changing the subject parameter ($U_{t,wall,construction}$, $U_{t,roof,construction}$, $U_{door,construction}$, $U_{window,construction}$) increases the number of air changes per hour (*ACH*). The value of the subject parameters ($U_{t,wall,construction}$, $U_{t,roof,construction}$, $U_{door,construction}$, $U_{window,construction}$) is changed from 0 W/m^2.K to 8 W/m^2.K. It is important to mention here is that this minimum and the maximum value ($U_{t,wall,construction}$, $U_{t,roof,construction}$, $U_{door,construction}$, $U_{window,construction}$) is purely hypothetical because an overall heat transfer coefficient value of 0 W/m^2.K would be too less (even impossible) and a value of 8 W/m^2.K would be too high for different elements of the building envelope. However, this range is selected for the simulation purposes in which the actual heat transfer coefficient would exist somewhere between 0.1 W/m^2.K to 3 W/m^2.K. It is noted that the increase in all of the subject variables ($U_{t,wall,construction}$, $U_{t,roof,construction}$, $U_{door,construction}$, $U_{window,construction}$) increases the number of air changes until reaching a critical point of <2 W/m^2.K after which it remains constant. In the physical process, the increase in the variables ($U_{t,wall,construction}$, $U_{t,roof,construction}$, $U_{door,construction}$, $U_{window,construction}$)increases the heat transmission capacity from the room to the outside of the building ($T_a > T_r$), resulting in the decrease of the room temperature. In other words, the internal heat generation is a source of heat, and increasing the variables ($U_{t,wall,construction}$, $U_{t,roof,construction}$, $U_{door,construction}$, $U_{window,construction}$) act as a sink of heat in the control volume. For smaller values of ($U_{t,wall,construction}$, $U_{t,roof,construction}$, $U_{door,construction}$, $U_{window,construction}$) i.e. <2 W/m^2.K, the difference between the fluid temperature and the room temperature ($T_f - T_r$) is relatively high, which favors the ventilation rate, and increases the *ACH* at the beginning, and remains constant afterward. It is also noted that changing the value of the variable ($U_{t,wall,construction}$) by eight times i.e. from 0 W/m^2.K to 8 W/m^2.K, only changes the *ACH* by ~0.8% i.e. ~1.23 1/h to ~1.24 1/h. Similarly, the *ACH* changes by only ~1.6% i.e., from ~1.23 1/h to 1.25 1/h, ~0.016% i.e., from ~1.2302 1/h to 1.2304 1/h, and ~0.8% i.e., from ~1.22 1/h to ~1.23 1/h, for $U_{t,roof,construction}$, $U_{door,construction}$ and $U_{window,construction}$, respectively.

Fig. A. 3. (e, h, n, and q) shows the same trend in which changing the subject parameter ($U_{t,wall,construction}$, $U_{t,roof,construction}$, $U_{door,construction}$, $U_{window,construction}$)decreases the energy efficiency until the critical point <2 W/m^2.K after which it remains constant. Lower values of the variables ($U_{t,wall,construction}$, $U_{t,roof,construction}$, $U_{door,construction}$, $U_{window,construction}$) restrict the heat transmission from the building envelope which increases the outlet fluid temperature $T_{f,o}$. The energy efficiency changes from ~30.57% to 29.57% (percentage change of ~3.27%) by increasing $U_{t,wall,construction}$ by around 8 times. The energy efficiency changes from ~30.42% to 28.96% (percentage change of ~4.79%) by increasing $U_{t,roof,construction}$ by around 8 times. The energy efficiency changes from ~30.62% to 30.61% (percentage change of ~0.03%) by increasing $U_{door,construction}$ by around 8 times. The energy efficiency changes from ~30.70% to 30.58% (percentage change of ~0.39%) by increasing $U_{window,construction}$ by around 8 times.

Fig. A. 3. (f, i, o, and r) shows the same trend in which changing the subject parameter ($U_{t,wall,construction}$, $U_{t,roof,construction}$, $U_{door,construction}$, $U_{window,construction}$)increases the specific environmental influence (Ψ) until the critical point <2 W/m^2.K after which it remains constant. It is directly correlated with the increasing ventilation rate at the beginning caused by the temperature difference between the fluid and the room ($T_f - T_r$), consequently increasing the specific environmental influence (Ψ) and remaining constant afterward. The highly sensitive elements of the envelope have the following order: roof, walls, window, and door.

The behavior of changing $U_{t,floor,construction}$ on the performance indicators is a reverse trend as shown in Fig. A. 3. (j, k, and l). It is because the calculation of the overall heat transfer coefficient from the room to the floor does not involve the air temperature, instead of a ground temperature which is considered 18 °C for comparative analysis purposes. In this sense, a reciprocal of the physical phenomena happens as explained previously in the case of $U_{t,wall,construction}$, $U_{t,roof,construction}$, $U_{door,construction}$, $U_{window,construction}$. *ACH* decreases from ~1.22 1/h to ~1.17 1/h (a change of 4.09%), energy efficiency increases from 31.04% to 34.09% (a change of 9.82%), and specific environmental influence (Ψ) changes from 736.18 kg_{CO2e}/m^3/year to 706.15 kg_{CO2e}/m^3/year (a change of 4.07%) by changing $U_{t,floor,construction}$ from 0 W/m^2.K to 8 W/m^2.K.

In conclusion from this section, it can be said that the building envelope parameters and the occupant dynamics ($\dot{q}_{gen}$, $U_{t,wall,construction}$, $U_{t,roof,construction}$, $U_{t,floor,construction}$, $U_{door,construction}$, $U_{window,construction}$) are not highly sensitive with respect to the three performance indicators, and their selected value does not change the overall deductions and conclusions of the research design.

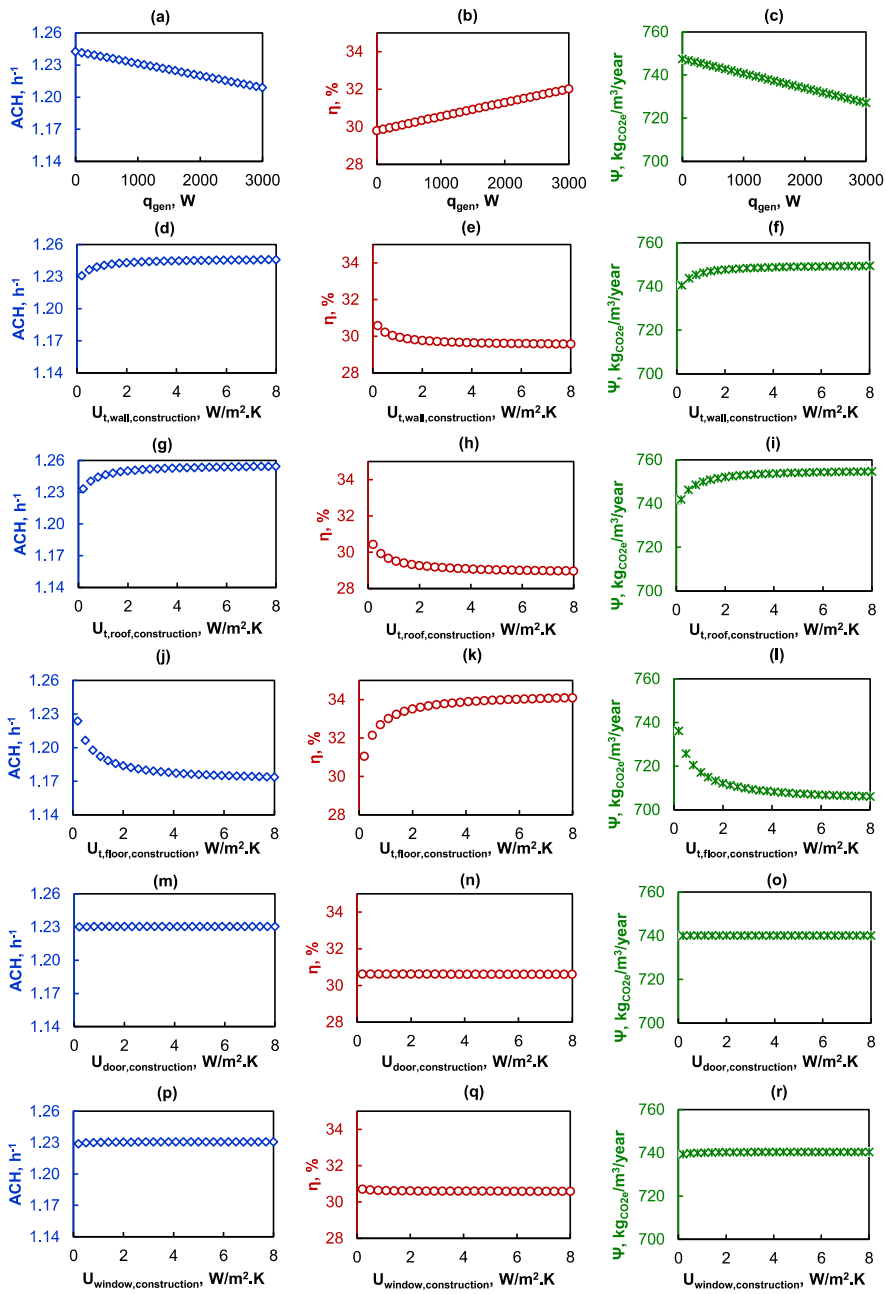

Fig. A. 3. Influence of internal heat generation ($\dot{q}_{gen}$) on (a) air changes per hour (ACH), (b) energy efficiency (η), and (c) specific environmental influence (Ψ). Influence of overall heat transfer coefficient of the construction of the wall ($U_{t,wall,construction}$) on (d) air changes per hour (ACH), (e) energy efficiency (η), and (f) specific environmental influence (Ψ). Influence of overall heat transfer coefficient of the construction of the roof ($U_{t,roof,construction}$) on (g) air changes per hour (ACH), (h) energy efficiency (η), and (i) specific environmental influence (Ψ). Influence of overall heat transfer coefficient of the construction of the floor ($U_{t,floor,construction}$) on (j) air changes per hour (ACH), (k) energy efficiency (η), and (l) specific environmental influence (Ψ). Influence of overall heat transfer coefficient of the construction of the door ($U_{door,construction}$) on (m) air changes per hour (ACH), (n) energy efficiency (η), and (o) specific environmental influence (Ψ). Influence of overall heat transfer coefficient of the construction of the window ($U_{window,construction}$) on (p) air changes per hour (ACH), (q) energy efficiency (η), and (r) specific environmental influence (Ψ).

Appendix B. MANOVA Tables for Multivariate Regression

See Table B. I.

Table B.I
Multivariate analysis of variance for estimation of **(a)** air changes per hour (ACH), **(b)** energy efficiency (η), and **(c)** specific environmental influence (Ψ).

(a)

Analysis of variance

Source	Sum of squares	Degree of freedom	Mean Square	F-test	p value	Comments
Model	4101.72	27	151.916	5794.97	0.0000	Significant
Residue	28.2861	1079	0.0262151			
Total	4130.01	1106				

(a1)

Parameter	Estimation	Standard error	T statistic	p value	Comments
L	−0.215852	0.0831898	−2.59469	0.0095	Significant
W	−0.567914	0.145953	−3.89108	0.0001	Significant
d	−3.94004	1.31744	−2.99069	0.0028	Significant
T_a	0.0053464	0.00267718	1.99703	0.0458	Significant
I_T	0.000648039	0.000762947	0.849389	0.3957	Not significant
v_{wind}	0.00823943	0.0887939	0.0927927	0.9261	Not significant
L^2	−0.0258362	0.00226782	−11.3925	0.0000	Significant
W^2	−0.0131572	0.00671384	−1.95972	0.0500	Not significant
d^2	−5.13382	0.566235	−9.06658	0.0000	Significant
T_a^2	−0.000009356	0.00000838113	−1.11632	0.2643	Not significant
I_T^2	−5.56726E-7	1.82203E-7	−3.05552	0.0022	Significant
v_{wind}^2	0.00105466	0.00267144	0.394792	0.6930	Not significant
$L\times\ W$	0.179655	0.00377689	47.567	0.0000	Significant
$L\times\ d$	1.16865	0.0335465	34.8366	0.0000	Significant
$L\times\ T$	0.000147408	0.000264883	0.5565	0.5779	Not significant
$L\times\ I_T$	0.000147119	0.000018101	8.12767	0.0000	Significant
$L\times\ v_{wind}$	−0.00212947	0.0022304	−0.954748	0.3397	Not significant
$W\times\ d$	2.95678	0.0588929	50.206	0.0000	Significant
$W\times\ T_a$	−0.0000558805	0.000458672	−0.121831	0.9030	Not significant
$W\times\ I_T$	0.000422529	0.0000317713	13.2991	0.0000	Significant
$W\times\ v_{wind}$	−0.00345675	0.0038275	−0.903134	0.3665	Not significant
$d\times\ T_a$	0.00260031	0.00409595	0.63485	0.5255	Not significant
$d\times\ I_T$	0.00240612	0.000291439	8.25602	0.0000	Significant
$d\times\ v_{wind}$	−0.0585279	0.0344745	−1.69772	0.0896	Not significant
$d\times\ I_T$	−0.00000272418	0.00000233736	−1.1655	0.2438	Not significant
$T_a\times\ v_{wind}$	0.00000988228	0.000285585	0.0346037	0.9724	Not significant
$I_T\times\ v_{wind}$	−0.00000983244	0.0000202489	−0.485579	0.6273	Not significant

(b)

Analysis of variance

Source	Sum of squares	Degree of freedom	Mean Square	F-test	p value	Comments
Model	926961.0	27	34331.9	960.57	0.0000	Significant
Residue	38564.6	1079	35.7411			
Total	965525.0	1106				

(b1)

Parameter	Estimation	Standard error	T statistic	p value	Comments
L	0.723375	3.0717	0.235497	0.8138	Not significant
W	0.31599	5.38915	0.0586345	0.9532	Not significant
d	−49.8892	48.645	−1.02558	0.3051	Not significant
T_a	−0.811394	0.0988521	−8.20815	0.0000	Significant
I_T	0.0206058	0.028171	0.731452	0.4645	Not significant
v_{wind}	9.33924	3.27862	2.84853	0.0044	Significant
L^2	0.152793	0.0837368	1.82468	0.0680	Not significant
W^2	−0.211285	0.247902	−0.852292	0.3940	Not significant
d^2	−8.22953	20.9076	−0.393614	0.6939	Not significant
T_a^2	0.00299734	0.000309465	9.68558	0.0000	Significant
I_T^2	0.0000154457	0.00000672766	2.29586	0.0217	Significant
v_{wind}^2	0.0966878	0.09864	0.980209	0.3270	Not significant
$L\times\ W$	0.159679	0.139458	1.145	0.2522	Not significant
$L\times\ d$	−2.30612	1.23867	−1.86177	0.0626	Not significant
$L\times\ T$	−0.00745861	0.00978055	−0.762596	0.4457	Not significant
$L\times\ I_T$	0.00100504	0.000668361	1.50374	0.1326	Not significant
$L\times\ v_{wind}$	−0.211589	0.0823552	−2.56922	0.0102	Significant
$W\times\ d$	1.48186	2.17456	0.681454	0.4956	Not significant
$W\times\ T_a$	−0.00250894	0.016936	−0.148142	0.8822	Not significant
$W\times\ I_T$	0.0000683109	0.00117312	0.05823	0.9536	Not significant
$W\times\ v_{wind}$	0.023907	0.141326	0.169161	0.8657	Not significant

(*continued on next page*)

Table B.I (*continued*)

(b1)

Parameter	Estimation	Standard error	T statistic	p value	Comments
$d \times T_a$	0.335815	0.151239	2.22043	0.0264	Significant
$d \times I_T$	−0.0675877	0.0107611	−6.28076	0.0000	Significant
$d \times v_{wind}$	3.26696	1.27293	2.56648	0.0103	Significant
$d \times I_T$	−0.0000944929	0.0000863045	−1.09488	0.2736	Not significant
$T_a \times v_{wind}$	−0.0339785	0.0105449	−3.22226	0.0013	Significant
$I_T \times v_{wind}$	−0.000315347	0.000747669	−0.421774	0.6732	Not significant

(c)

Analysis of variance

Source	Sum of squares	Degree of freedom	Mean Square	F-test	p value	Comments
Model	1.48438E9	27	5.4977E7	5794.97	0.0000	Significant
Residue	1.02365E7	1079	9487.02			
Total	1.49461E9	1106				

(c1)

Parameter	Estimation	Standard error	T statistic	p value	Comments
L	−129.851	50.0448	−2.59469	0.0095	Significant
W	−341.642	87.8013	−3.89108	0.0001	Significant
d	−2370.23	792.536	−2.99069	0.0028	Significant
T_a	3.21626	1.61052	1.99703	0.0458	Significant
I_T	0.389844	0.458969	0.849389	0.3957	Not significant
v_{wind}	4.95663	53.4161	0.0927927	0.9261	Not significant
L^2	−15.5424	1.36426	−11.3925	0.0000	Significant
W^2	−7.91505	4.03887	−1.95972	0.0500	Not significant
d^2	−3088.37	340.632	−9.06658	0.0000	Significant
T_a^2	−0.00562833	0.00504187	−1.11632	0.2643	Not significant
I_T^2	−0.000334912	0.000109609	−3.05552	0.0022	Significant
v_{wind}^2	0.634457	1.60707	0.394792	0.6930	Not significant
$L \times W$	108.076	2.27208	47.567	0.0000	Significant
$L \times d$	703.027	20.1807	34.8366	0.0000	Significant
$L \times T$	0.0886767	0.159347	0.5565	0.5779	Not significant
$L \times I_T$	0.088503	0.0108891	8.12767	0.0000	Significant
$L \times v_{wind}$	−1.28103	1.34175	−0.954748	0.3397	Not significant
$W \times d$	1778.72	35.4285	50.206	0.0000	Significant
$W \times T_a$	−0.0336162	0.275925	−0.121831	0.9030	Not significant
$W \times I_T$	0.254183	0.0191128	13.2991	0.0000	Significant
$W \times v_{wind}$	−2.07949	2.30252	−0.903134	0.3665	Not significant
$d \times T_a$	1.56428	2.46402	0.63485	0.5255	Not significant
$d \times I_T$	1.44746	0.175322	8.25602	0.0000	Significant
$d \times v_{wind}$	−35.2089	20.7389	−1.69772	0.0896	Not significant
$d \times I_T$	−0.0016388	0.00140609	−1.1655	0.2438	Not significant
$T_a \times v_{wind}$	0.00594492	0.1718	0.0346037	0.9724	Not significant
$I_T \times v_{wind}$	−0.00591494	0.0121812	−0.485579	0.6273	Not significant

Appendix C. Nomenclature

See Table C.I.

Table C.I
Nomenclature of the letters, symbols, and subscripts used in the physical model.

Letters	
A	Area, m^2
A_o	Outlet area of solar chimney, m^2
A_i	Inlet area of solar chimney, m^2
A_r	Area ratio, -
ACH	Number of air changes per hour, 1/h
C_d	Coefficient of discharge of air channel, -
c_f	Specific heat of fluid, J/kg.K
d	Distance from the glass to the wall, m
$EF_{electricity}$	Emission factor of electricity, kg_{CO2e}/kWh
g	Gravitational acceleration, m/s^2
Gr	Grashof number, -
h_c	Convective heat transfer coefficient, $W/m^2.K$
h_r	Radiative heat transfer coefficient, $W/m^2.K$
h_{wind}	Convective heat transfer coefficient because of wind, $W/m^2.K$

(*continued on next page*)

Table C.I (*continued*)

I_T	Total incident solar radiation, W/m^2
I_b	Beam solar radiation, W/m^2
I_d	Diffused incident solar radiation, W/m^2
k_f	Thermal conductivity of fluid, W/m.K
L	Length (vertical height) of the solar chimney, m
$\dot{m}$	Mass flow rate, kg/s
Nu	Nusselt number, -
Pr	Prandtl number, -
P_s	Static pressure, Pa
$\dot{q}_{gen}$	Heat generation, W
R_b	Tilt factor, -
Ra	Rayleigh number, -
S	Total absorbed solar radiation, W/m^2
T	Temperature, K
T_{ground}	Ground temperature, K
U_t	Overall/total heat transfer coefficient, W/m^2.K
$\dot{V}$	Volumetric flow rate, m^3/s
v_{wind}	Wind velocity, m/s
W	Width (amplitude) of solar chimney, m
Δw	Width, m
Symbols	
ρ_g	Ground reflectance, -
β	Tilt angle, degrees
ϕ	Latitude, degrees
δ	Declination angle, degrees
ω	Hour angle, degrees
σ	Stefan-Boltzmann constant, W/m^2.K^4
α	Absorptivity, -
ε	Emissivity, -
τ	Transmissivity, -
η	Efficiency, %
β_f	Thermal expansion coefficient of fluid, 1/K
ν	Kinematic viscosity, m^2/s
η_{fan}	Fan efficiency, %
ϖ	Equivalent shaft power, kW
Ψ	Specific environmental influence, kg$_{CO2e}$/m^3/year
Subscripts	
a	Ambient
g	Glass
w	Wall
f	Fluid

Appendix D. Supplementary data

Supplementary data to this article can be found online at https://doi.org/10.1016/j.buildenv.2022.108807.

References

[1] B. Wen, S.N. Musa, C.C. Onn, S. Ramesh, L. Liang, W. Wang, K. Ma, The role and contribution of green buildings on sustainable development goals, Build. Environ. 185 (2020) 107091, https://doi.org/10.1016/J.BUILDENV.2020.107091.

[2] M. Sarkhosh, A.A. Najafpoor, H. Alidadi, J. Shamsara, H. Amiri, T. Andrea, F. Kariminejad, Indoor Air Quality associations with sick building syndrome: an application of decision tree technology, Build. Environ. 188 (2021) 107446, https://doi.org/10.1016/J.BUILDENV.2020.107446.

[3] M. Awada, B. Becerik-Gerber, E. White, S. Hoque, Z. O'Neill, G. Pedrielli, J. Wen, T. Wu, Occupant health in buildings: impact of the COVID-19 pandemic on the opinions of building professionals and implications on research, Build. Environ. 207 (2022) 108440, https://doi.org/10.1016/J.BUILDENV.2021.108440.

[4] T.L. Yip, Y. Huang, C. Liang, Built environment and the metropolitan pandemic: analysis of the COVID-19 spread in Hong Kong, Build, Environ. Times 188 (2021) 107471, https://doi.org/10.1016/J.BUILDENV.2020.107471.

[5] A.M. Hassan, N.A. Megahed, COVID-19 and urban spaces: a new integrated CFD approach for public health opportunities, Build. Environ. 204 (2021) 108131, https://doi.org/10.1016/J.BUILDENV.2021.108131.

[6] Y.L. Li, M.Y. Han, S.Y. Liu, G.Q. Chen, Energy consumption and greenhouse gas emissions by buildings: a multi-scale perspective, Build. Environ. 151 (2019) 240–250, https://doi.org/10.1016/J.BUILDENV.2018.11.003.

[7] P. Pallis, K. Braimakis, T.C. Roumpedakis, E. Varvagiannis, S. Karellas, L. Doulos, M. Katsaros, P. Vourliotis, Energy and economic performance assessment of efficiency measures in zero-energy office buildings in Greece, Build. Environ. 206 (2021) 108378, https://doi.org/10.1016/J.BUILDENV.2021.108378.

[8] F. Mostafavi, M. Tahsildoost, Z.S. Zomorodian, Energy efficiency and carbon emission in high-rise buildings: a review (2005-2020), Build. Environ. 206 (2021) 108329, https://doi.org/10.1016/J.BUILDENV.2021.108329.

[9] H. Teixeira, M.G. Gomes, A. Moret Rodrigues, J. Pereira, Thermal and visual comfort, energy use and environmental performance of glazing systems with solar control films, Build. Environ. 168 (2020) 106474, https://doi.org/10.1016/J.BUILDENV.2019.106474.

[10] A.M. Raimundo, N.B. Saraiva, A.V.M. Oliveira, Thermal insulation cost optimality of opaque constructive solutions of buildings under Portuguese temperate climate, Build. Environ. 182 (2020) 107107, https://doi.org/10.1016/J.BUILDENV.2020.107107.

[11] Y. Cao, S. Pourhedayat, H.S. Dizaji, M. Wae-hayee, A comprehensive optimization of phase change material in hybrid application with solar chimney and photovoltaic panel for simultaneous power production and air ventilation, Build. Environ. 197 (2021) 107833, https://doi.org/10.1016/J.BUILDENV.2021.107833.

[12] H. Kitagawa, T. Asawa, T. Kubota, A.R. Trihamdani, H. Mori, Thermal storage effect of radiant floor cooling system using phase change materials in the hot and humid climate of Indonesia, Build. Environ. 207 (2022) 108442, https://doi.org/10.1016/J.BUILDENV.2021.108442.

[13] S. Kashyap, J. Sarkar, A. Kumar, Development and experimental analysis of a novel dual-mode counter-flow evaporative cooling device, Build. Environ. 205 (2021) 108176, https://doi.org/10.1016/J.BUILDENV.2021.108176.

[14] C. Wang, Q. Wang, B. Nourozi, H. Pieskä, A. Ploskić, Evaluating the cooling potential of a geothermal-assisted ventilation system for multi-family dwellings in

the Scandinavian climate, Build. Environ. 204 (2021) 108114, https://doi.org/10.1016/J.BUILDENV.2021.108114.
[15] A. Jankovic, F. Goia, Impact of double skin facade constructional features on heat transfer and fluid dynamic behaviour, Build. Environ. 196 (2021) 107796, https://doi.org/10.1016/J.BUILDENV.2021.107796.
[16] G. He, Q. Wu, Z. Li, W. Ge, D. Lv, L. Cong, Ventilation performance of solar chimney in a test house: field measurement and validation of plume model, Build. Environ. 193 (2021) 107648.
[17] S. Sivalakshmi, M. Raja, R. Mahudeswaran, G. Gowtham, Thermal performance of wall solar chimney integrated with a room under warm and humid conditions, Mater. Today Proc. 43 (2021) 1892–1895, https://doi.org/10.1016/J.MATPR.2020.10.833.
[18] H. Zhang, Y. Tao, K. Nguyen, F. Han, J. Li, L. Shi, A wall solar chimney to ventilate multi-zone buildings, Sustain. Energy Technol. Assessments 47 (2021) 101381, https://doi.org/10.1016/J.SETA.2021.101381.
[19] A. Vazquez-Ruiz, J.M.A.M.A. Navarro, J.F.F. Hinojosa, J.P.P. Xamán, Effect of the solar roof chimney position on heat transfer in a room, Int. J. Mech. Sci. 209 (2021) 106700, https://doi.org/10.1016/J.IJMECSCI.2021.106700.
[20] Y. Cao, F. Aldawi, N. Sinaga, H. Moria, H.S. Dizaji, M. Wae-hayee, Single solar chimney technology as a natural free ventilator; energy-environmental case study for Hong Kong, Case Stud. Therm. Eng. 26 (2021) 101173, https://doi.org/10.1016/J.CSITE.2021.101173.
[21] A. Soto, P.J. Martínez, P.J. Martínez, J.A. Tudela, Simulation and experimental study of residential building with north side wind tower assisted by solar chimneys, J. Build. Eng. 43 (2021) 102562.
[22] M.M. Villar-Ramos, E.V. Macias-Melo, K.M. Aguilar-Castro, I. Hernández-Pérez, J. Arce, J. Serrano-Arellano, H.P. Díaz-Hernández, L.M. López-Manrique, Parametric analysis of the thermal behavior of a single-channel solar chimney, Sol. Energy 209 (2020) 602–617.
[23] A. Salari, M. Ashouri, A. Hakkaki-Fard, On the performance of inclined rooftop solar chimney integrated with photovoltaic module and phase change material: a numerical study, Sol. Energy 211 (2020) 1159–1169, https://doi.org/10.1016/J.SOLENER.2020.10.064.
[24] Y. Cao, N. Sinaga, S. Pourhedayat, H.S. Dizaji, Innovative integration of solar chimney ventilator, solar panel and phase change material; under real transient weather condition of Hong Kong through different months, Renew. Energy 174 (2021) 865–878, https://doi.org/10.1016/J.RENENE.2021.04.146.
[25] F. Pouranian, H. Akbari, S.M. Hosseinalipour, Performance assessment of solar chimney coupled with earth-to-air heat exchanger: a passive alternative for an indoor swimming pool ventilation in hot-arid climate, Appl. Energy 299 (2021) 117201, https://doi.org/10.1016/J.APENERGY.2021.117201.
[26] H. Wang, C. Lei, Theoretical modeling of combined solar chimney and water wall for buildings, Energy Build. 187 (2019) 186–200, https://doi.org/10.1016/j.enbuild.2019.01.025.
[27] Y. Li, T. Long, X. Bai, L. Wang, W. Li, S. Liu, J. Lu, Y. Cheng, K. Ye, S. Huang, An experimental investigation on the passive ventilation and cooling performance of an integrated solar chimney and earth–air heat exchanger, Renew. Energy 175 (2021) 486–500, https://doi.org/10.1016/J.RENENE.2021.05.004.
[28] L. Shi, A. Ziem, G. Zhang, J. Li, S. Setunge, Solar chimney for a real building considering both energy-saving and fire safety – a case study, Energy Build. 221 (2020) 110016.
[29] X. Cheng, L. Shi, P. Dai, G. Zhang, H. Yang, J. Li, Study on optimizing design of solar chimney for natural ventilation and smoke exhaustion, Energy Build. 170 (2018) 145–156, https://doi.org/10.1016/J.ENBUILD.2018.04.016.
[30] X. Cheng, Z. Shi, K. Nguyen, L. Zhang, Y. Zhou, G. Zhang, J. Wang, L. Shi, Solar chimney in tunnel considering energy-saving and fire safety, Energy 210 (2020) 118601, https://doi.org/10.1016/J.ENERGY.2020.118601.
[31] N. Zhu, R. Deng, P. Hu, F. Lei, L. Xu, Z. Jiang, Coupling optimization study of key influencing factors on PCM trombe wall for year thermal management, Energy 236 (2021) 121470, https://doi.org/10.1016/J.ENERGY.2021.121470.
[32] Q. Ma, H. Fukuda, X. Wei, A. Hariyadi, Optimizing energy performance of a ventilated composite Trombe wall in an office building, Renew. Energy 134 (2019) 1285–1294, https://doi.org/10.1016/J.RENENE.2018.09.059.
[33] A.A. Serageldin, A.K. Abdelrahman, S. Ookawara, Parametric study and optimization of a solar chimney passive ventilation system coupled with an earth-to-air heat exchanger, Sustain. Energy Technol. Assessments 30 (2018) 263–278, https://doi.org/10.1016/j.seta.2018.10.010.
[34] L. Shi, G. Zhang, An empirical model to predict the performance of typical solar chimneys considering both room and cavity configurations, Build. Environ. 103 (2016) 250–261, https://doi.org/10.1016/J.BUILDENV.2016.04.024.
[35] A. Salehi, R. Fayaz, M. Bozorgi, S. Asadi, V. Costanzo, N. Imani, F. Nocera, Investigation of thermal comfort efficacy of solar chimneys under different climates and operation time periods, Energy Build. 205 (2019) 109528, https://doi.org/10.1016/j.enbuild.2019.109528.
[36] S. Jamali, A. Nemati, F. Mohammadkhani, M. Yari, Thermal and economic assessment of a solar chimney cooled semi-transparent photovoltaic (STPV) power plant in different climates, Sol. Energy 185 (2019) 480–493, https://doi.org/10.1016/J.SOLENER.2019.04.073.
[37] I. Hernández-López, J. Xamán, I. Zavala-Guillén, I. Hernández-Pérez, P. Moreno-Bernal, Y. Chávez, Thermal performance of a solar façade system for building ventilation in the southeast of Mexico, Renew. Energy 145 (2020) 294–307, https://doi.org/10.1016/j.renene.2019.06.026.
[38] C. Jiménez-Xamán, J. Xamán, M. Gijón-Rivera, I. Zavala-Guillén, F. Noh-Pat, E. Simá, Assessing the thermal performance of a rooftop solar chimney attached to a single room, J. Build. Eng. 31 (2020) 101380, https://doi.org/10.1016/j.jobe.2020.101380.
[39] D. Garson, Interpreting neural-network connection weights, AI Expet. 6 (1991) 46–51. https://dl.acm.org/doi/10.5555/129449.129452. (Accessed 14 August 2021).
[40] R. Tariq, N.A. Sheikh, J. Xamán, A. Bassam, An innovative air saturator for humidification-dehumidification desalination application, Appl. Energy 228 (2018) 789–807, https://doi.org/10.1016/j.apenergy.2018.06.135.
[41] ASHRAE, ANSI/ASHRAE Standard 62.1: Ventilation for Acceptable Indoor Air Quality, 2013. Atlanta, https://www.ashrae.org/technical-resources/bookstore/standards-62-1-62-2. (Accessed 11 July 2021).
[42] T. Miyazaki, A. Akisawa, T. Kashiwagi, The effects of solar chimneys on thermal load mitigation of office buildings under the Japanese climate, Renew. Energy 31 (2006) 987–1010, https://doi.org/10.1016/j.renene.2005.05.003.
[43] H. Wan, T. Cao, Y. Hwang, S.O. Andersen, S. Chin, A comprehensive review of life cycle climate performance (LCCP) for air conditioning systems, Int. J. Refrig. (2021), https://doi.org/10.1016/J.IJREFRIG.2021.06.026.
[44] A.D. Belegundu, T.R. Chandrupatla, Optimization Concepts and Applications in Engineering, second ed., Cambridge University Press, 2011 https://doi.org/10.1017/CBO9780511975905.
[45] S. Baluja, R. Caruana, Removing the genetics from the standard genetic algorithm, in: ICML'95 Proc. Twelfth Int. Conf. Int. Conf. Mach. Learn., 1995, pp. 1–10.
[46] K. Deb, A. Pratap, S. Agarwal, T. Meyarivan, A fast and elitist multiobjective genetic algorithm: NSGA-II, IEEE Trans. Evol. Comput. 6 (2002) 182–197, https://doi.org/10.1109/4235.996017.
[47] MATLAB, Gamultiobj Algorithm. https://www.mathworks.com/help/gads/gamultiobj-algorithm.html#brjtxfv-1, 2021. (Accessed 9 August 2021).
[48] MathWorks, The Language of Technical Computing, 2017. https://www.mathworks.com/products/matlab.html.
[49] STATGRAPHICS Centurion. https://www.statgraphics.com/, 2021. (Accessed 11 May 2021).
[50] M. Mahbobi, T.K. Tiemann, Introductory Business Statistics with Interactive Spreadsheets, first ed., BCcampus, 2015. https://opentextbc.ca/introductorybusinessstatistics/front-matter/about-the-book/. (Accessed 11 August 2021).
[51] Neural Net Fitting Tool, 2006. https://www.mathworks.com/help/deeplearning/ref/nftool.html#d123e145896. (Accessed 10 August 2021).
[52] M. Fasihi, R. Weiss, J. Savolainen, C. Breyer, Global potential of green ammonia based on hybrid PV-wind power plants, Appl. Energy 294 (2021) 116170, https://doi.org/10.1016/J.APENERGY.2020.116170.
[53] J. Ascencio-Vásquez, K. Brecl, M. Topič, Methodology of Köppen-Geiger-Photovoltaic climate classification and implications to worldwide mapping of PV system performance, Sol. Energy (2019), https://doi.org/10.1016/j.solener.2019.08.072.
[54] R. Tariq, N.A. Sheikh, A. Livas-García, J. Xamán, A. Bassam, V. Maisotsenko, Projecting global water footprints diminution of a dew-point cooling system: sustainability approach assisted with energetic and economic assessment, Renew. Sustain. Energy Rev. 140 (2021), https://doi.org/10.1016/j.rser.2021.110741.
[55] M. Safi, Death Toll Climbs in Karachi Heatwave, Guard. News Media, 2018. https://www.theguardian.com/world/2018/may/22/death-toll-climbs-in-karachi-heatwave. (Accessed 13 August 2021).
[56] M. Mashal, Heat-related Mortality in India: Excess All-Cause Mortality Associated with the 2010 Ahmedabad Heat Wave, New York Times, 2019, p. 9. https://www.nytimes.com/2019/06/13/world/asia/india-heat-wave-deaths.html. (Accessed 13 August 2021).
[57] Worldometer, Countries in the World by Population, 2020, 2020, https://www.worldometers.info/world-population/population-by-country/.
[58] forecast to 2025, Global Air Conditioner Market 2020 by Manufacturers, Regions, Type and Application, 2020, https://www.industryresearch.biz/TOC/15445584#TOC.
[59] I.B. Ruiz, How to prevent cooling from warming up the world, Dtsch. Welle. (2018). https://www.dw.com/en/how-to-prevent-cooling-from-warming-up-the-world/a-44734986. (Accessed 11 March 2021).
[60] D. Ürge-Vorsatz, L.F. Cabeza, S. Serrano, C. Barreneche, K. Petrichenko, Heating and cooling energy trends and drivers in buildings, Renew. Sustain. Energy Rev. 41 (2015), https://doi.org/10.1016/j.rser.2014.08.039.
[61] REN21, Renewables 2018, Global Status Report, REN21 Secretariat), Paris, 2018.
[62] J.A. Duffie, W.A. Beckman, Solar Engineering of Thermal Processes, fourth ed., John Wiley & Sons, New York, USA, 2013.
[63] F.P. Incropera, D.P. Dewitt, T.L. Bergman, A.S. Lavine, Fundamentals of Heat and Mass Transfer, John Wiley & Sons, 2007, https://doi.org/10.1016/j.applthermaleng.2011.03.022.
[64] W.H. McAdams, Heat Transmission, 1954, https://doi.org/10.1021/ie50031a003.
[65] T. Ma, J. Zhao, Z. Li, Mathematical modelling and sensitivity analysis of solar photovoltaic panel integrated with phase change material, Appl. Energy 228 (2018) 1147–1158, https://doi.org/10.1016/j.apenergy.2018.06.145.
[66] K.S. Ong, A mathematical model of a solar chimney, Renew. Energy (2003), https://doi.org/10.1016/S0960-1481(02)00057-5.
[67] J. Arce, J.P. Xamn, G. Lvarez, M.J. Jiménez, R. Enrquez, M.R. Heras, A simulation of the thermal performance of a small solar chimney already installed in a building, J. Sol. Energy Eng. Trans. ASME. 135 (2013), https://doi.org/10.1115/1.4007088.
[68] B. Belfegas, S. Larbi, T. Tayebi, Experimental and theoretical investigation on a solar chimney system for ventilation of a living room, Math. Model. Eng. Probl. 8 (2021) 259–266, https://doi.org/10.18280/mmep.080213.
[69] J. Martí-Herrero, M.R. Heras-Celemin, Dynamic physical model for a solar chimney, Sol. Energy 81 (2007) 614–622, https://doi.org/10.1016/j.solener.2006.09.003.

[70] J. Hirunlabh, W. Kongduang, P. Namprakai, J. Khedari, Study of natural ventilation of houses by a metallic solar wall under tropical climate, Renew. Energy 18 (1999) 109–119, https://doi.org/10.1016/S0960-1481(98)00783-6.
[71] J. Lucero-álvarez, N.A. Rodríguez-Muñoz, I.R. Martín-Domínguez, The effects of roof and wall insulation on the energy costs of low income housing in Mexico, Sustain. Times 8 (2016) 1–19, https://doi.org/10.3390/su8070590.
[72] C.K. Romero-Pérez, N.A. Rodríguez-Muñoz, M.G. Alpuche-Cruz, I.R. Martín-Domínguez, Preliminary study of the condition of social housing in the city of Durango, México, Energy Procedia 134 (2017) 29–39, https://doi.org/10.1016/j.egypro.2017.09.594.
[73] I.R. Martin-Dominguez, N.A. Rodriguez-Muñoz, C.K. Romero-Perez, M. Najera-Trejo, N. Ortega-Avila, Analysis of the methodologic assumptions of the NOM-020-ENER-2011—mexican residential building standard, Environ. - MDPI. 5 (2018) 1–18, https://doi.org/10.3390/environments5110118.
[74] A.C. Borbon-Almada, N.A. Rodriguez-Muñoz, M. Najera-Trejo, Energy and economic impact on the application of low-cost lightweight materials in economic housing located in dry climates, Sustain. Times 11 (2019), https://doi.org/10.3390/su11061586.
[75] A.C. Borbon-Almada, J. Lucero-Alvarez, N.A. Rodriguez-Muñoz, M. Ramirez-Celaya, S. Castro-Brockman, N. Sau-Soto, M. Najera-Trejo, Design and application of cellular concrete on a mexican residential building and its influence on energy savings in hot climates: projections to 2050, Appl. Sci. 10 (2020) 1–22, https://doi.org/10.3390/app10228225.
[76] N.A. Rodríguez Muñoz, Evaluation of the thermal performance of construction systems to reduce the energy consumption in buildings: a case study in a cold semi-arid climate, Acta Univ. 30 (2020) 1–18, https://doi.org/10.15174/au.2020.2941.
[77] ASHRAE, ASHRAE Climatic Design Conditions 2009/2013/2017, ASHRAE, 2017. http://ashrae-meteo.info/.
[78] World Bank Group, Global Wind Atlas, 2021. https://globalwindatlas.info/. (Accessed 7 August 2021).
[79] Ministry of Housing Communities & Local Government, United Kingdom, the Future Buildings Standard: Consultation on Changes to Part L (Conservation of Fuel and Power), Building Regulations for Non-domestic Buildings and Dwellings; and Overheating in New, 2021. England, https://www.gov.uk/government/publications/building-regulations-approved-documents-l-f-and-overheating-consultation-version. (Accessed 28 July 2021).
[80] R. Forest, World Cities by Climate Zone, 2020. https://storymaps.arcgis.com/stories/345bc9c775d1424280b776ec38c3b1e1. (Accessed 7 August 2021).
[81] J. Mathur, S. Mathur, Anupma, Summer-performance of inclined roof solar chimney for natural ventilation, Energy Build. 38 (2006) 1156–1163, https://doi.org/10.1016/J.ENBUILD.2006.01.006.
[82] J. Mathur, N.K. Bansal, S. Mathur, M. Jain, Anupma, Experimental investigations on solar chimney for room ventilation, Sol. Energy 80 (2006) 927–935, https://doi.org/10.1016/J.SOLENER.2005.08.008.
[83] N.K. Bansal, J. Mathur, S. Mathur, M. Jain, Modeling of window-sized solar chimneys for ventilation, Build. Environ. 40 (2005) 1302–1308, https://doi.org/10.1016/J.BUILDENV.2004.10.011.
[84] O. May Tzuc, A. Bassam, L.J. Ricalde, O.A. Jaramillo, M. Flota-Bañuelos, M. A. Escalante Soberanis, Environmental-economic optimization for implementation of parabolic collectors in the industrial process heat generation: case study of Mexico, J. Clean. Prod. 242 (2020) 118538, https://doi.org/10.1016/j.jclepro.2019.118538.
[85] S. Haykin, Neural Networks and Learning Machines, third ed., Pearson, Ontario Canada, 2001 third ed. https://www.pearson.com/us/higher-education/program/Haykin-Neural-Networks-and-Learning-Machines-3rd-Edition/PGM320370.html. (Accessed 10 August 2021).
[86] A.H. Elsheikh, S.W. Sharshir, M. Abd Elaziz, A.E. Kabeel, W. Guilan, Z. Haiou, Modeling of solar energy systems using artificial neural network: a comprehensive review, Sol. Energy 180 (2019) 622–639, https://doi.org/10.1016/J.SOLENER.2019.01.037.
[87] O. May Tzuc, A. Livas-García, M. Jiménez Torres, E. Cruz May, L.M. López-Manrique, A. Bassam, Artificial intelligence techniques for modeling indoor building temperature under tropical climate using outdoor environmental monitoring, J. Energy Eng. 146 (2020), 04020004, https://doi.org/10.1061/(ASCE)EY.1943-7897.0000649.
[88] O.M. Tzuc, A. Bassam, F. Anguebes-Franseschi, L.J. Ricalde, M. Flota-Bañuelos, M. C. Téllez, Multivariate optimization applied for the economic competitiveness analysis of photothermal systems into industrial heat production: an approach based on artificial intelligence, J. Renew. Sustain. Energy 12 (2020), 055501, https://doi.org/10.1063/5.0016142.
[89] O. May Tzuc, O. Rodríguez Gamboa, R. Aguilar Rosel, M. Che Poot, H. Edelman, M. Jiménez Torres, A. Bassam, Modeling of hygrothermal behavior for green facade's concrete wall exposed to nordic climate using artificial intelligence and global sensitivity analysis, J. Build. Eng. 33 (2021) 101625, https://doi.org/10.1016/J.JOBE.2020.101625.
[90] E. Cruz May, A. Bassam, L.J. Ricalde, M.A. Escalante Soberanis, O. Oubram, O. May Tzuc, A.Y. Alanis, A. Livas-García, Global sensitivity analysis for a real-time electricity market forecast by a machine learning approach: a case study of Mexico, Int. J. Electr. Power Energy Syst. 135 (2022) 107505, https://doi.org/10.1016/J.IJEPES.2021.107505.